A contribution to the quantification of crustal shortening and kinematics of deformation across the Western Andes (~20–22°S).

Tania Habel[1], Martine Simoes[1], Robin Lacassin[1], Daniel Carrizo[2,3], German Aguilar[2]

[1] Université Paris Cité, Institut de physique du globe de Paris, CNRS, F-75005 Paris, France

[2] Advanced Mining Technology Center, Facultad de Ciencias Físicas y Matemáticas, Universidad de Chile, Avenida Tupper 2007, Santiago, Chile

[3] now at GeoEkun SpA, Santiago 7500593, Chile

Correspondence to: Martine Simoes (simoes@ipgp.fr)

Abstract. The Andes are an emblematic active Cordilleran orogen. Mountain-building in the Central Andes (~20°S) started by Late Cretaceous to Early Cenozoic along the subduction margin, and propagated eastward. In general, the structures sustaining the uplift of the western flank of the Andes are dismissed, and their contribution to mountain-building remains poorly constrained. Here, we focus on two sites along the Western Andes at ~20–22°S, in the Atacama Desert, where structures are well exposed. We combine mapping from high-resolution satellite images with field observations and numerical trishear forward modeling to provide quantitative constraints on the kinematic evolution of the investigated field sites. When up-scaling our local field interpretations to the regional scale, we identify two main structures: (1) the Andean Basement Thrust, a west-vergent thrust system placing Andean Paleozoic basement over Mesozoic strata; and (2) a series of west-vergent thrusts pertaining to the West Andean Thrust System, deforming primarily Mesozoic units. From our interpreted sections, we estimate that both structures accommodate together at least ~6–9 km of shortening across the sole investigated ~7–17 km-wide field sites. This multi-kilometric shortening represents only a fraction of the total shortening accommodated across the whole Western Andes. The timing of the main deformation recorded in the folded Mesozoic series can be bracketed between ~68 and ~29 Ma – and possibly between ~68 and ~44 Ma – from dated deformed geological layers, with a subsequent significant slowing-down of shortening rates. Even though the structures forming the Western Andes only absorbed a small fraction of the total shortening across the whole orogen, their contribution has been relatively significant at the earliest stages of Andean mountain-building, before deformation proceded eastward.

1 Introduction

Along the western margin of South America (Figure 1), the oceanic Nazca plate plunges beneath the South American continent, with a present-day convergence rate of ~8 cm/yr at ~20°S, according to the NUVEL-1A model (Demets et al., 1994). The subduction megathrust absorbs most of this convergence in the form of large earthquakes (magnitude Mw ≥ 8). A small fraction of it – presently ~1 cm/yr at 20°S (e.g. Norabuena et al., 1998; Brooks et al., 2011) – contributes to the deformation of the
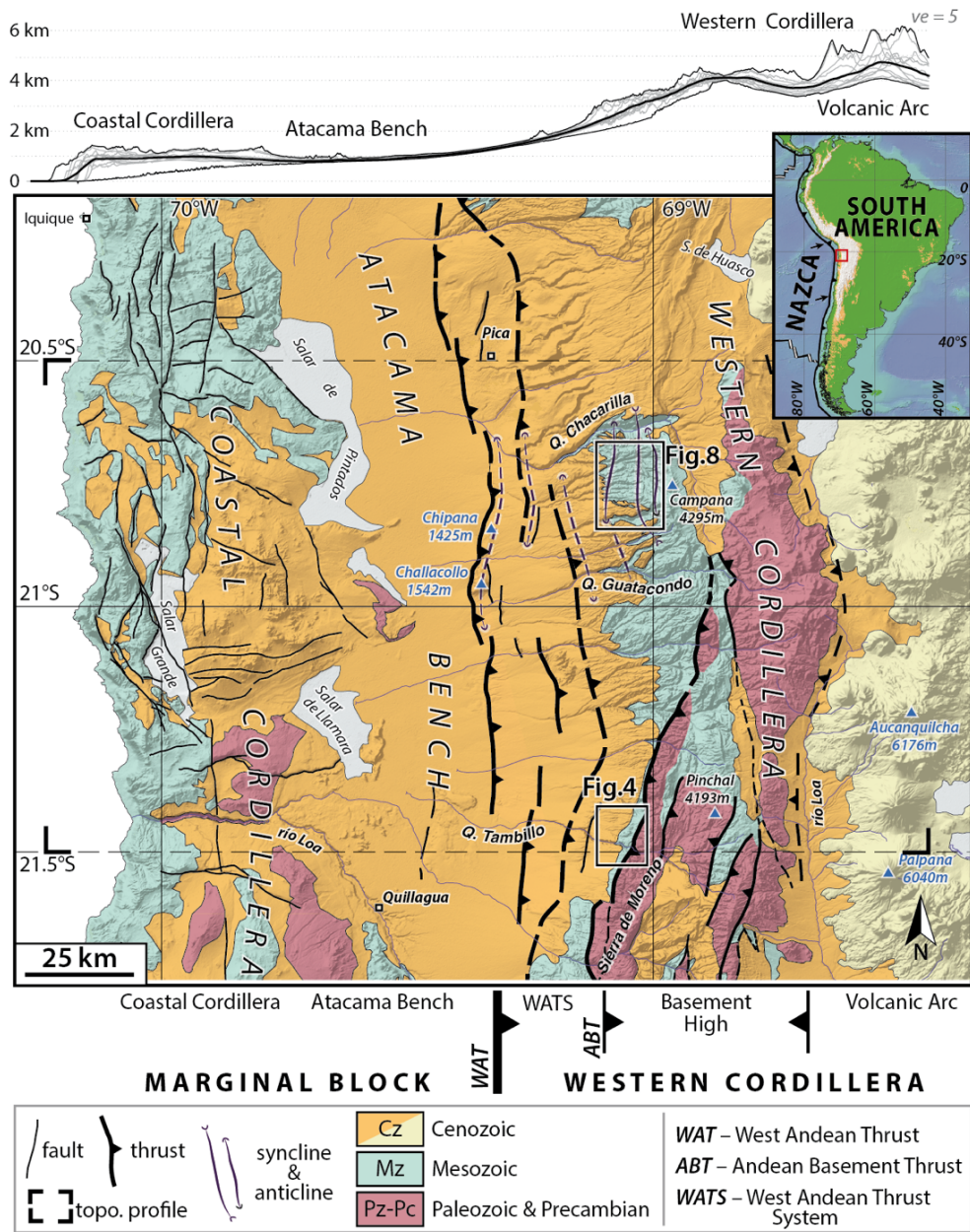
Figure 1. Simplified geological and structural map of the Western Central Andes at ~20–22°S (Northern Chile) and average topographic profile. Map modified from Armijo et al. (2015), vertical exaggeration (ve) of 5 for topographic profile. The Marginal Block and the Western Cordillera constitute the two main structural ensembles. The Western Cordillera includes the West Andean Thrust System (WATS), a basement high (Cordillera Domeyko), and the modern volcanic arc. The structures forming the WATS are mostly hidden beneath blanketing Cenozoic deposits and only outcrop in few places. The Andean Basement Thrust separates the basement high of the Western Cordillera from the WATS. The locations of Figures 4 (Pinchal area) and 8 (Quebrada Blanca area) are reported. Inset: Location of the map (red box) within the South American Continent.

upper plate over millions of years and to the formation of one of the largest reliefs at the Earth's surface: the Andean Cordilleras and the Altiplano-Puna Plateau in between.

Andean mountain-building initiated by Late Cretaceous-Early Cenozoic along the Western Andes of the Bolivian Orocline (between 16–22°S), and proceeded since then with the progressive eastward propagation of deformation onto the South
45   American continent (e.g. Armijo et al., 2015; Charrier et al., 2007; Decelles et al., 2014; Eichelberger et al., 2013; Oncken et al., 2006; Jaillard et al., 2000; and references therein). Most local and mountain-wide studies have essentially focused on the Altiplano-Puna plateau and on the various cordilleras to the east. In comparison, the structures located along the western flank of the orogen have remained up to now relatively under-studied.

In most classical models of Andean mountain-building, the western flank is described as a passive monoclinal-like crustal-
50   scale flexure (e.g., Isacks, 1988; Lamb, 2011, 2016; Mcquarrie, 2002). However, in the late 1980's, Mpodozis et al. (1989) described west-vergent thrusting along the Western Andean margin. Later, other authors also described various thrusts, mostly west-vergent (but not only) (e.g. Charrier et al., 2007; Farías et al., 2005; Fuentes et al., 2018; Garcia and Hérail, 2005; Martinez et al., 2021; Muñoz and Charrier, 1996; Victor et al., 2004), but they generally gave these thrusts a minor role in the building of the western flank of the orogen. Only further south, at the latitude of Santiago de Chile (~33°30'S), a clear west-vergent
55   fold-and-thrust-belt has been documented along the Western Andes (Armijo et al., 2010; Riesner et al., 2017; Riesner et al., 2018). This thrust belt emerges at the active San Ramon Fault in front of the capital city of Santiago de Chile, and has absorbed a relatively significant amount of crustal shortening (Riesner et al., 2017; Riesner et al., 2018).

At 33°30'S, the orogen is relatively young and narrow. In contrast, ~1300 km further north, at ~20–22°S where the Andes-Altiplano system is much wider and structurally more complex, the contribution of structures along the Western Andes is
60   probably small compared to the >300 km total shortening (e.g. Anderson et al., 2017; Barnes and Ehlers, 2009; Eichelberger et al., 2013; Elger et al., 2005; Kley and Monaldi, 1998; Mcquarrie et al., 2005; Sheffels, 1990) across the entire >650 km wide orogen, but their role at the onset of orogenic building may have been significant (Armijo et al., 2015). One of the difficulties in better quantifying the contribution of these structures is that a large part of the deformation is hidden under blanketing mid-upper Cenozoic deposits and volcanics (Figure 1) (Armijo et al., 2015; Farías et al., 2005; Sernageomin, 2003;
65   Victor et al., 2004). A quantitative analysis of this deformation and its kinematics is only possible at the few sites along the western flank where deformed Mesozoic series crop out and which are accessible despite the hostile desert conditions in North Chile.

In this study, we provide quantitative structural data to better constrain the geometry of structures, the shortening they accommodated and their kinematics of deformation over time in two of the few areas along the West Andean flank where the
70   underlying deformed Mesozoic layers are exposed (Figure 1). The Pinchal area, at ~21°30'S, exhibits a west-vergent thrust that brings the Paleozoic basement of the Cordillera Domeyko over folded Mesozoic units. In the Quebrada Blanca zone, ~80 km further north, the excellent exposure of folded Mesozoic series allows for a more quantitative estimate of the shortening and of the timing of the main deformation episode. These two study areas only give a limited view on the deformation of the whole Western Andean flank (Figure 1). Despite these limitations, we find that the shortening of these structures is multi-

kilometric, revealing that the contribution of the West Andean flank to Andean mountain building is not negligible. Additionally, we show that the main deformation recorded by the folded Mesozoic units occurred sometime between ~68 and ~29 Ma (and possibly between ~68 Ma and ~44 Ma), further emphasizing that these structures mostly participated to the early stages of mountain-building.

2 Geological Context of the Central Andes (~20–22°S)

2.1 General geological framework

At ~20–22°S, from west to east, the Andean margin (Figure 1) is constituted of: (1) the subduction margin, including the Peru–Chile Trench, the oceanward forearc, and the Coastal Cordillera that reaches elevations >1 km and that corresponds to the former Mesozoic volcanic arc; (2) the Atacama Bench or Central Depression, at an altitude of ~1 km, corresponding to a modern continental forearc basin, well expressed in the morphology and topography of North Chile; and (3) the strictly speaking Andean orogen (e.g. Charrier et al., 2007; Mcquarrie et al., 2005; Oncken et al., 2006). The morpho-tectonic units located west of the Andean orogen constitute the Marginal Block (i.e. the oceanward forearc, the Coastal Cordillera and the Atacama Bench; Figure 1) (Armijo et al., 2015; Armijo et al., 2010).

At ~20–22°S latitude, the Andes are characterized by their largest width (>650 km), highest average elevation (~4–4.5 km above sea level, hereafter a.s.l., Figure 1), thickest crust (70–80 km, e.g. Heit et al., 2007; Tassara et al., 2006; Wölbern et al., 2009; Yuan et al., 2000; Zandt et al., 1994) and greatest total shortening (>300 km, e.g. Anderson et al., 2017; Barnes and Ehlers, 2009; Eichelberger et al., 2013; Elger et al., 2005; Kley and Monaldi, 1998; Mcquarrie et al., 2005; Sheffels, 1990). Here, the Andean orogen is composed, from west to east, of: (1) the Western Cordillera, including the Cordillera Domeyko and the modern volcanic arc (Figure 1) (e.g. Armijo et al., 2015; Eichelberger et al., 2013; Garzione et al., 2017; Mcquarrie, 2002; Oncken et al., 2006); (2) the Altiplano Plateau, a high-elevation internally drained low-relief basin; (3) the Eastern Cordillera (or Cordillera Oriental); (4) the Interandean zone; and (5) the Subandean ranges, east of which the South American craton underthrusts the Andes (e.g. Armijo et al., 2015; Isacks, 1988; Mcquarrie et al., 2005; Oncken et al., 2006).

The building of the Andean mountain-belt *stricto sensu* proceeded since the Late Cretaceous - Early Cenozoic at ~20–22°S and was associated with crustal shortening and thickening (e.g. Armijo et al., 2015; Charrier et al., 2007; Decelles et al., 2014; Eichelberger et al., 2013; Oncken et al., 2006; Jaillard et al., 2000; and references therein). Based on regional syntheses (e.g. Armijo et al., 2015; Charrier et al., 2007; Garzione et al., 2017; Horton, 2018; Mcquarrie et al., 2005; Oncken et al., 2006), the across-strike growth of the orogen is summarized as follows: (1) by Late Cretaceous, the Mesozoic arc and backarc basin (formed during the early Andean cycle) was located at the position of the present-day forearc, and most of the Andes showed mainly flat topography; (2) by Late Cretaceous - Early Cenozoic, orogenic growth initiated primarily along the western margin of the present-day Altiplano; (3) by ~45–30 Ma, shortening vanished along the western flank of the Andes, and was transferred to the Eastern Cordillera; (4) by ~25 Ma, deformation ended in the Eastern Cordillera and migrated to the Interandean Belt; (5) from ~10 Ma until present, deformation within the Subandean Belt proceeded with the underthrusting of the Brazilian

Craton beneath the Andes. It is therefore clear that the Andean shortening started along the Western Andes and subsequently propagated eastward, progressively enlarging the orogen to form the different cordilleras and the Altiplano plateau in between.

2.2 Geological setting of the western flank of the Andes at ~20–22°S

110 The Andean western flank is formed of three tectono-stratigraphic units at ~20–22°S, aside from the present-day volcanic arc. These units are hereafter described following a stratigraphic logic, starting from the oldest and deepest units exposed to the east at higher altitudes, to the youngest units observed mostly to the west at lower altitudes (Figure 1). These units are: (1) the Andean basement consisting of metamorphic rocks of Precambrian and Paleozoic ages; (2) the folded volcano-sedimentary deposits of Mesozoic age (Triassic–Cretaceous), unconformably overlain by (3) less-deformed mid-upper Cenozoic

115 (Oligocene – Quaternary) volcanics and sedimentary cover (Sernageomin, 2003). Magmatic intrusions locally alter these different units, and are mostly Cenozoic. This only pictures the first-order structuration of the Western Andean flank, as Mesozoic strata may be locally trapped in between two basement units, and Cenozoic layers may be unconformably overlying older strata even to the east (Figure 1). Laterally, and in particular further south (i.e. south of the city of Calama, ~22°27'), the structural organization of the western flank of the Andes is more complex, most probably because of the variable lateral

120 structuration of the earlier Mesozoic Andean basins, and the description proposed here does not directly apply.

2.2.1 Stratigraphic and geologic background

The pre-Andean basement rocks formed during the Late Proterozoic and Paleozoic, when the Amazonian craton was progressively assembled from various terranes (e.g. Charrier et al., 2007; Lucassen et al., 2000; Ramos, 1988; Rapela et al., 1998). At the end of this period of subduction and continental accretion, intense magmatic activity (volcanism and major

125 granite intrusions) welded together the basement during the Late Carboniferous to Early Permian (Charrier et al., 2007; Ramos, 1988; Vergara and Thomas, 1984).

The Mesozoic deposits (Triassic to Cretaceous), found today along the West Andean flank, formed in a proto-Andean arc and backarc basin system during the early period of the Andean cycle (e.g. Charrier et al., 2007; Mpodozis et al., 1989). Marine and continental sediments are interbedded with volcano-magmatic rocks (Aguilef et al., 2019; Sernageomin, 2003). These

130 Mesozoic units attain locally thicknesses up to ≥10 km (e.g. Buchelt and Cancino, 1988; Charrier et al., 2007; Mpodozis et al., 1989).

A regional erosional surface called the Choja Pediplain (Galli-Olivier, 1967) developed during the Eocene to Early Oligocene (~50–30 Ma) (e.g. Armijo et al., 2015; Victor et al., 2004; and references therein). Above this angular unconformity, the up to ~1600 m thick (Labbé et al., 2019) Cenozoic deposits of the Altos de Pica Formation are composed of continental clastic

135 sediments, interbedded with volcanic layers (Victor et al., 2004). The oldest documented age within the Altos de Pica Formation is of ~24–26 Ma from dated ignimbrites (Farías et al., 2005; Victor et al., 2004). From there, an age of ~27–29 Ma for the base of the formation is inferred regionally when extrapolated to the basal erosional surface. The youngest ignimbrites within the Altos de Pica Formation are dated at ~14–17 Ma (Middle Miocene) (Vergara and Thomas, 1984; Victor et al., 2004).

From there and from other younger dated ignimbrites (Baker, 1977; Vergara and Thomas, 1984), Victor et al. (2004) deduced
140 from stratigraphic correlations that the development of the Altos de Pica Formation finished by ~5–7 Ma (Late Miocene) at
~20–22ºS.

2.2.2 Structural and kinematic context

The Paleozoic basement of the Western Cordillera is disrupted at places in the form of various basement highs boarded by
reverse faults (e.g. Haschke and Gunther, 2003; Henriquez et al., 2019; Puigdomenech et al., 2020; Tomlinson et al., 2001)
145 (Figure 1) – not to be confused with the north–south trending strike-slip Domeyko Fault System, also called West Fissure
System (e.g. Charrier et al., 2007; Reutter et al., 1996; Tomlinson and Blanco, 1997b; Tomlinson and Blanco, 1997a), east and
out of our field study area. At ~20-22°S, various maps describe west-vergent thrusts in overall structural continuity, bringing
the Paleozoic basement westward over folded Mesozoic units (Aguilef et al., 2019; Haschke and Gunther, 2003; Sernageomin,
2003; Skarmeta and Marinovic, 1981). Using apatite fission track dating, Maksaev and Zentilli (1999) proposed significant
150 exhumation of the basement units between 50 Ma and 30 Ma, possibly related to basement overthrusting. Older exhumation
ages (Late Cretaceous to Early Cenozoic (U-Th)/He zircon and apatite ages) are however provided by Reiners et al. (2015) for
the Western Andean basement at ~21°42'S, but from only one sample and without modeling. Together, these ages indicate
that data remain missing to better quantify the exhumation, uplift and timing of deformation of the basement thrusts reported
along this part of the Western Andean flank.
155 Further west, a series of mostly west-vergent thrusts have been inferred, essentially from seismic profiles. These thrusts result
from the tectonic inversion of the previous Mesozoic basins, and affect the Mesozoic to Cenozoic series (Fuentes et al., 2018;
Martinez et al., 2021; Victor et al., 2004; Armijo et al., 2015). Victor et al. (2004) determined ~3 km of shortening of the syn-
tectonic Altos de Pica Formation layers, but they did not take into account the deformation of the underlying more deformed
Mesozoic units. Other authors propose limited shortening on these older deeper layers (Fuentes et al., 2018; Martinez et al.,
160 2021), but the poor quality of the seismic profiles at these depths renders these interpretations quite tenuous and disputable.
Haschke and Gunther (2003) estimated that >9 km of shortening across the western flank in the outcropping Sierra de Moreno
area (~21°45'S) occurred since the Late Cretaceous to Eocene on a west- and east-verging thrust system. Whether these various
faults are connected at depth onto an east-dipping master fault (Armijo et al., 2015; Haschke and Gunther, 2003; Victor et al.,
2004) or whether their are steeply dipping single planar faults (Fuentes et al., 2018; Martinez et al., 2021) remains debated:
165 these considerations are nowhere documented by data and only rely on a priori concepts or structural reasonings at a larger
regional scale. It follows that even if published data document the existence of various faults along the Western Andean front
at ~20–22°S, their geometry, kinematics and total amount of shortening have not yet been satisfactorily evaluated.

3 Data and Methods

Unconformable slightly deformed mid-upper Cenozoic clastic sediments and ignimbrites commonly hide the folded Mesozoic
170 layers and their contact with the basement (Figure 1). Field investigations are limited to the few sparse areas where the erosion
of the Cenozoic cover has exposed the underlying structures (Aguilef et al., 2019; Sernageomin, 2003). In this study, we focus
on two relatively accessible outcrop sites (Figure 1): (1) at ~21°30'S, where the Paleozoic basement overthrusts Mesozoic
units (Skarmeta and Marinovic, 1981). This zone will be referred to as the Pinchal area (next to Cerro Pinchal, 4193 m a.s.l.).
(2) At ~20°45'S, where folded Mesozoic units can be observed. This zone is hereafter named Quebrada Blanca area, after its
175 largest canyon.

3.1 Available Data

The most detailed - even though large-scale - existing geological map for the Pinchal area is the 1:250,000 Quillagua map
(Skarmeta and Marinovic, 1981). For the Quebrada Blanca area, the recent 1:100,000 Guatacondo map (Blanco and
Tomlinson, 2013) provides detailed and updated information on the stratigraphy and structure. There, the structure of the
180 folded Mesozoic rocks has been preliminarily mapped and qualitatively described by other authors (Armijo et al., 2015; Blanco
and Tomlinson, 2013; Fuentes et al., 2018).

Enhanced cartographic details can be deduced from high-resolution satellite imagery. We use Google Earth imagery (Landsat
7, DigitalGlobe) whose resolution varies from a few meters to a few tens of meters depending on the zones. In addition, this
work benefits from very high-resolution imagery from the European Pléiades satellites. Using the MicMac software suite
185 (Rosu et al., 2014; Rupnik et al., 2016), we calculate high-resolution DEMs from tri-stereo Pléiades imagery, with a 0.5 m
resolution. These DEMs are down-sampled to a resolution of 2 m to enhance data treatment and calculations (e.g. stratigraphic
projection and image processing). Relative vertical accuracy may reach ~1 m, depending on local slope.

Field observations were acquired during two field surveys in March 2018 and January 2019. Difficult accessibility and field
logistics in the remote and desert Pinchal area only allow detailed complementary field observations on a relatively limited
190 area. Observation points and the off-road track followed to reach our field site in the Pinchal area are provided as supplementary
material.

3.2 Structural maps

To establish structural maps, we do 3D-mapping of stratigraphic layers, after Armijo et al. (2010) and Riesner et al. (2017).
Layers are traced and correlated on Google Earth satellite images. The so-obtained georeferenced traces are projected on the
195 DEM-derived topographic map to obtain their altitude, and on geological maps for stratigraphic referencing. Field observations
allow ground verifications and provide supplementary details, such as minor thrusts and folds, the observation of polarity
criteria or local dip angles.

The approach used here is mainly limited by local geological complications. Continuous mapping of Mesozoic strata is locally complicated where incision of Cenozoic strata is limited, where magmatic intrusions and associated hydrothermalism alter the structural geometries, where layers with no well-expressed bedding such as marls are present (ex: Pinchal area), or where landslides or recent sediment deposits hide the underlying deformation pattern. Therefore, geometrical observations and detailed mapping of the structures may be locally difficult, in some zones impossible. These difficulties cause some uncertainties in precisely correlating mapped layers, but only result in limited metric to decametric errors and do not modify our large-scale (km) results and interpretations.

3.3 Structural cross-sections

We use structural measurements, field observations and the obtained structural map to propose surface cross-sections across the two investigated areas.

In the Pinchal area, because of limited canyon incision, marls, and frequent blanketing of the structures by Cenozoic cover, we build our structural surface cross-sections mainly from field observations (strike and dip angles, polarity criteria, first-order stratigraphic column), with additional information taken from satellite imagery.

In contrast, in the Quebrada Blanca area, we build our surface cross-section mostly from mapping on satellite imagery. Here, we follow the approach proposed in Armijo et al. (2010) and described in detail in Riesner et al. (2017). The mapped georeferenced horizons are projected on the high-resolution Pléiades DEMs. Using a 3D-modeler, we project these layers along swath profiles chosen where Mesozoic strata crop out the best, where folds appear cylindrical and where topographic relief is most significant. This approach allows for getting more precisely the large-scale structural geometries by averaging the usual local minor variations in strikes and dips that derive from multiple field measurements. From there, we successfully obtain the overall sectional geometry of folded layers, and by comparing with the structural map, we determine the approximate locations of the major synclinal and anticlinal axes. By respecting the classical rule of constant layer thickness, we derive fold geometries.

We recognize the difficulty of unambiguously correlating stratigraphic layers in some cases, and the fact that layers may not keep constant thicknesses. As local topographic relief is reduced to a few hundred meters at most, the construction of surface cross-sections is mostly restricted to extrapolating derived average surface dip angles at depth. However, the main limitation relies on the fact that we can only draw the sub-surface sectional geometry of folds from surface geology. Indeed, we do not have from field observations any constraints on the geometry of the associated thrusts at depth, nor on the footwall structure of these thrusts. We propose a possible structural interpretation at depth and discuss its implications.

3.4 Crustal shortening and kinematic modeling

We apply a line-length-balancing approach to the obtained surface cross-sections to determine shortening related to folding only. This result is independent of the geometry of the associated faults at depth, does not account neither for penetrative deformation nor for slip on underlying faults, and stands here as a conservative minimum.

230 From surface geology, we have no precise indication on the structure and geometry of faults and layers at depth, in particular within the footwall of the inferred faults. To make a step forward in our estimates of crustal shortening, we consider the simplest structural geometries where underlying thrusts are parallel to the anticlinal backlimbs and root at least at the base of the folded series. From there, we model anticlinal geometries using a numerical trishear approach (e.g. (Allmendinger, 1998; Erslev, 1991)). We use the code FaultFold Forward (version 6) (Allmendinger, 1998) in order to jointly model thrust

235 displacement and anticlinal folding. Trishear models the deformation distributed within a triangular zone located at the tip of a propagating fault (Erslev, 1991). This forward modeling relies on testing a set of parameters, namely: the position of the fault tip, the angle of the propagating fault ramp, the slip on the fault, the propagation-to-slip-ratio (P/S) of the fault, the angle of the triangular zone at the tip of the fault where distributed deformation occurs (i.e. the trishear angle), and the inclined shear angle controlling the backlimb kinematics. We assume here the case of linear symmetric trishear to keep models as simple as

240 possible, meaning that folding of the backlimb occurs parallel to the fault. Initial layers are assumed to be sub-horizontal, with a slight eastward tilt (3°E at Quebrada Tambillo, 2°E at Quebrada Blanca) as expected in the initial Andean basin. We tested various combinations of parameters, within the range considered in the literature (e.g. Allmendinger, 1998; Allmendinger and Shaw, 2000; Cristallini and Allmendinger, 2002; Hardy and Ford, 1997; Zehnder and Allmendinger, 2000), and with regards to our field observations such as the possible geometry of faults at depth as constrained from surface geology. Parameters are

245 adjusted by trial and error to visually fit observed and interpreted structural geometries. By adding sedimentary layers at various steps during ongoing deformation, with initial geometries similar to the present-day regional topographic slope, we model syntectonic deposition and subsequent deformation, in order to reproduce deformation of Cenozoic layers. Additional information on trishear modeling (initial conditions, values of tested parameters, etc) are provided later and in supplementary material (Text S1, Tables S1-S3). We recognize that parameters of our preferred model may not be unique. This is not expected

250 to impact much estimated total shortening, as this result depends mostly on the modeled cross-sections (and therefore on the structural interpretation to be modeled) rather than on the preferred set of parameters. For instance, we cannot discard the possibility that faults are steeper and root deeper. If this were the case, crustal shortening would be lower.

Deformation is expressed in terms of shortening (in km) and of relative shortening at the scale of the investigated sites (in %). Relative shortening is hereafter defined as the ratio of the estimated shortening by the initial length of the undeformed section.

255 **4 Basement thrust and deformed Mesozoic series at Pinchal (~21º30'S)**

Because our observations are in contradiction with previous stratigraphic and structural interpretations of the folded Mesozoic series, we hereafter describe in detail our field observations. We subsequently discuss and compare them to previous interpretations, and propose a solution reconciling these observations with regional stratigraphic knowledge.
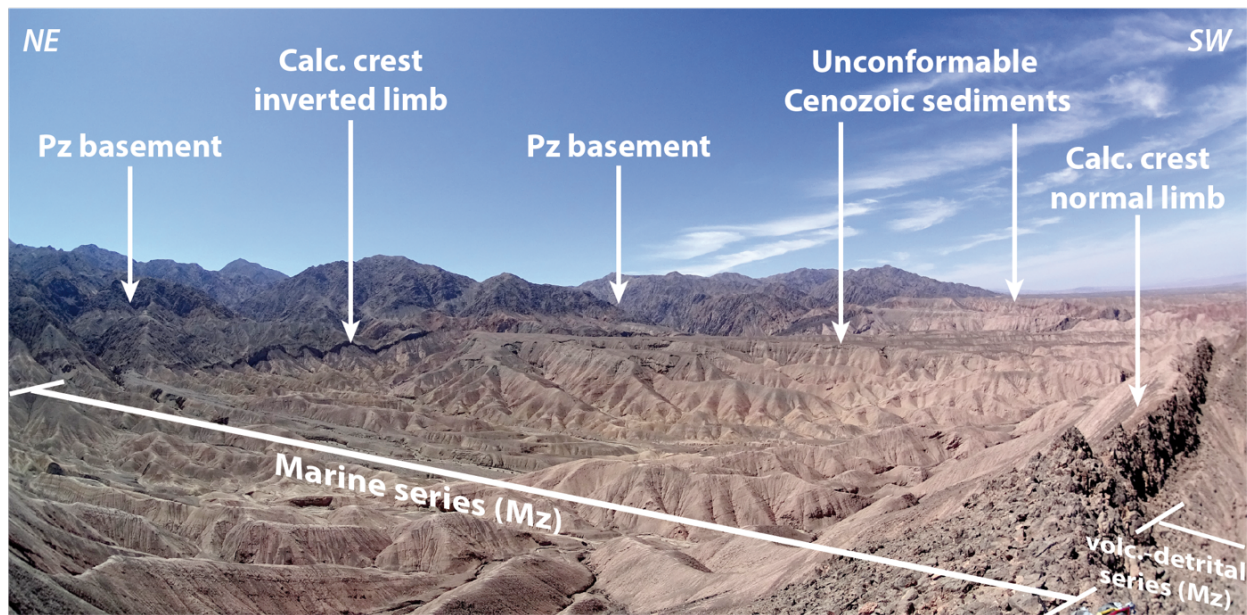
Figure 2. Landscape field view of the Pinchal area depicting the main tectono-stratigraphic units. The Paleozoic (Pz) basement stands clearly out in the background, characterized by its darker color and higher elevations. The Mesozoic (Mz) series in the central part and in the foreground bear a marine part and a volcano-detrital part, respectively, separated by an outstanding calcareous (Calc.) crest. Unconformable Cenozoic erosional surfaces, with limited fluvial deposits can also be observed.

4.1 Stratigraphic observations

In the landscape (Figure 2), the three main tectono-stratigraphic units are : (1) the metamorphic basement, (2) the Mesozoic sedimentary series (with a continuum from continental upward to marine facies), and (3) the continental Cenozoic cover. From field observations, we propose a first-order stratigraphic column (Figure 3). Field pictures of sedimentary formations are provided in supplementary material (Figures S1-S12) to complement the forthcoming descriptions. We acknowledge not to have any constraint on the absolute ages of these series, but the relative stratigraphic ages are deduced from the kilometer-scale structural geometry and from clear sedimentary or structural polarity criteria observed in the field. Thicknesses are inferred only locally, and thickness variations cannot be excluded.

The Paleozoic basement (Figure S1) dominates the eastern part of the Pinchal area, and is composed of mainly coarse-grain granodiorites and diorites, as well as metamorphic rocks comprising gneisses, migmatites and mica-schists, consistent with previous descriptions in the area (Skarmeta and Marinovic, 1981).

The older part of the outcropping Mesozoic series consists of continental deposits, with a high content of Paleozoic lithics and volcano-clastic and tuffitic low-rounded conglomerates, of greenish, beige and brownish colors (Figure S2). Clast sizes vary from a few millimeters to a few decimeters. At places, these rocks bear sedimentary polarity criteria such as grain-sorting, cross-bedding and tangential beds (Figure S3). In the eastern part of the Pinchal area, we locally observe below this series dark green detrital pelites (lutites) (Figure S4). On the basis of petrographic and sedimentological correlations, these detrital
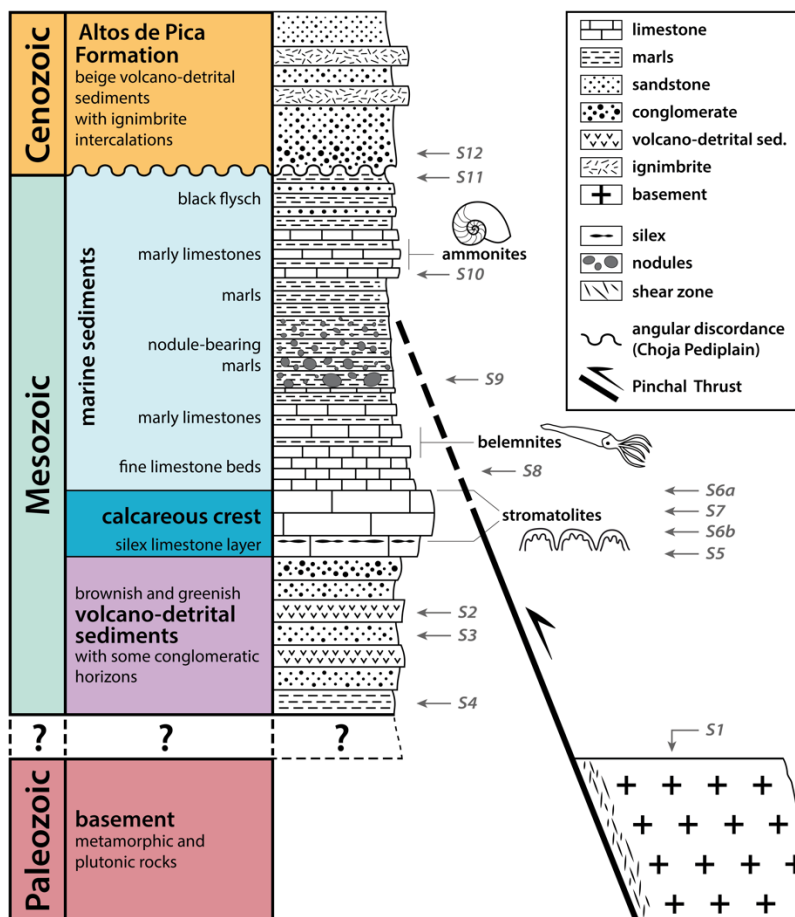
Figure 3. First-order stratigraphic column of the Pinchal area. Data are derived from field observations, mainly obtained along Quebrada Tania (Figures 4 and 5a). The column only depicts the stratigraphic succession, and thicknesses are not at scale (see text for information on thicknesses). The description of Cenozoic units is here completed based on the work of Victor et al. (2004). Color-code in line with maps (Figures 1, 4 and S14) and cross-sections (Figure 5). The Paleozoic basement overthrusts folded Mesozoic series along the Pinchal Thrust, so that part of the deeper and older Mesozoic series may be missing here. See main text and Figures S1–S12 in supplementary material for detailed sedimentologic descriptions.

Mesozoic sediments recall units mapped as Triassic north of the Pinchal zone (between 21°–21°30'S) in the Quehuita area (Aguilef et al., 2019).

In paraconformity, a characteristic limestone layer marks the beginning of a marine sequence, evidencing a marine transgression. We refer to this layer as the "calcareous crest" as it is prominent in the landscape (Figure 2) and can be easily used as a reference layer in the field or on satellite images. The base of the calcareous crest is characterized by silex layers or nodules (Figure S5). Upsection, numerous stromatolites (Figure S6) and bivalves (Figure S7) are found. Its thickness varies between a few meters (less than 10 m) in the eastern part, to ~10–20 m to the west.

The calcareous crest is overlain by thin-bedded (cm–dm) limestone layers of rose-beige color (Figure S8), over a thickness of ~50–100 m. Going up-section, the marine series becomes more marly, more beige, and with less limestone layers, evidencing

a deeper marine paleo-environment. Belemnite fossils were encountered in the lower part of this limestone-to-marl sequence. Characteristic calcareous oval concretions of variable diameter (cm to m) (Figure S9), are pervasive at the transition from

300 marly limestones to marls. The marls bear ammonites, which we have not precisely identified. These ammonites could be Perisphinctes, Euaspidoceras, Mirosphinctes and Gregoryceras, according to the notice of the Quillagua geological map (Skarmeta and Marinovic, 1981) if applicable here. In this case they would be of Middle Jurassic age (Bajocian to Callovian). The series from the thin-bedded limestones to the top of the beige marls is ~200 m thick along one of the canyons (Quebrada Tania).

305 Upsection, the beige marls become more calcareous again, with thin limestone layers (Figure S10). Finally, this marine sequence ends with black marls containing layers of beige sandstones (mm to few cm – rarely dm – thick) (Figure S11), indicative of a detrital component in a probable deep-seated basin, comparable to the "flysch" series of the Alpine basins (Homewood and Lateltin, 1988). This unit is hereafter called "black flysch", and has a minimum thickness of ~50 m. Continental-clastic Cenozoic deposits (Altos de Pica Formation), unconformably overlie this folded Mesozoic series, over the

310 Choja erosional surface (Galli-Olivier, 1967; Victor et al., 2004) (Figures 2 and 3). They are mainly composed of alluvial fan deposits sourced from the mountain front immediately to the east, locally interlayered or covered by ignimbrites. We encountered red arenites at the base of the Cenozoic series in the western part of the Pinchal area (Figure S12). The age of the oldest sedimentary deposits above this erosional surface is regionally inferred to be ~27–29 Ma (Victor et al., 2004) (see also section 2.2).

4.2 Structural observations

315

A structural map of the area is built after satellite and field observations (Figure 4). Two ~east–west cross-sections show detailed surface observations along two accessible representative canyons: Quebrada Tania and Quebrada Martine (Figures 5a,b). The Quebrada Tambillo incises deeper into folded units, so that surface structural observations can be further extrapolated at depth (Figure 5c).

320 The easternmost part of our study area is marked by a west-vergent thrust bringing the metamorphic basement over folded Mesozoic units (Figures 2, 4 and 6a). This basement thrust is hereafter named the Pinchal Thrust. The C/S-fabric ("Cisaillement/Schistosité") observed within the thrust shear zone indicates top-to-the-west thrusting (Figure 6b). The Pinchal Thrust roughly follows a north-south direction (Figure 4). This contact often resumes to a single basement thrust (Figures 5a,c), but may also show local geometrical complexities, with secondary thrusts and branches, eventually involving basement

325 with stripes of trapped Mesozoic units, as along Quebrada Martine (Figure 5b).
Folded Mesozoic units are observable west of the Pinchal Thrust (Figures 2 and 4). From east to west, an asymmetric and overturned syncline (Figure 7a) is followed by a relatively symmetric anticline (Figure 7b).
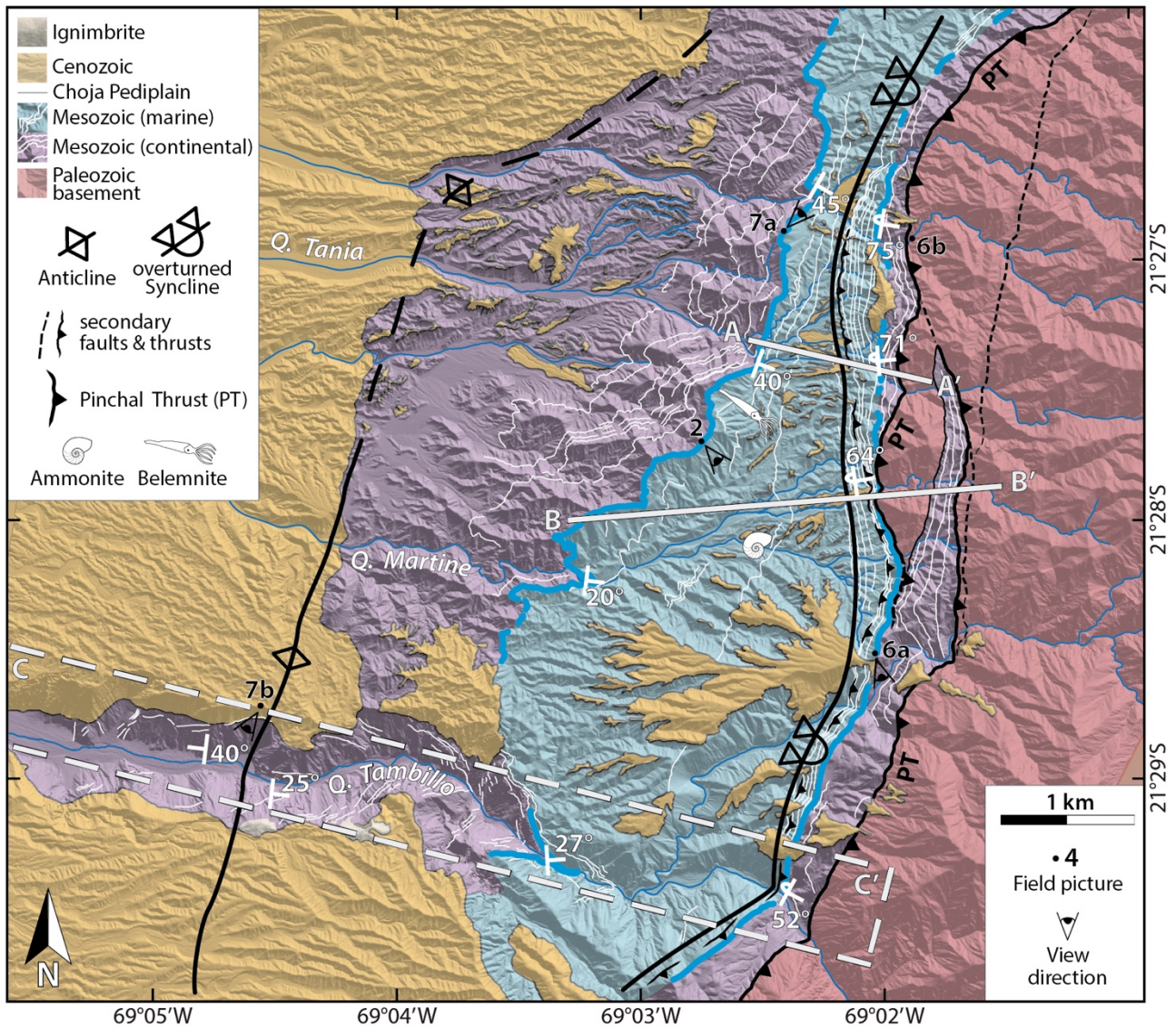
Figure 4. Structural map of the Pinchal area (location on Figure 1). White thin lines highlight Mesozoic layers mappable on satellite images. Thick blue line depicts the calcareous crest, which is used as a marker layer (Figure 2). A–A' and B–B' segments locate the surface cross-sections of Quebrada Tania and Quebrada Martine, respectively (Figures 5a-b). In the case of the Quebrada Tambillo cross-section, a topographic swath profile was used along C–C' (dashed box). The fold axes are relatively well defined for the synclinal fold, but less well constrained for the anticlinal fold because only observable along Quebrada Tambillo. Field pictures are numbered according to the corresponding figures. Background hillshaded DEM produced from tri-stereo Pléiades imagery. Q: Quebrada (Spanish word for "canyon").

The eastern limb of the syncline is inverted and locally highly faulted and folded (Figures 5 and S13). Within this inverted limb, the series goes westward (and upsection) from sheared lutites beneath the Pinchal Thrust, followed by Mesozoic detrital series with conglomerates, to the Mesozoic marine series from the calcareous crest upsection to the marly limestones. The overturned strata dip steeply (50–70ºE). Penetrative small-scale deformation is observed pervasively within the marine
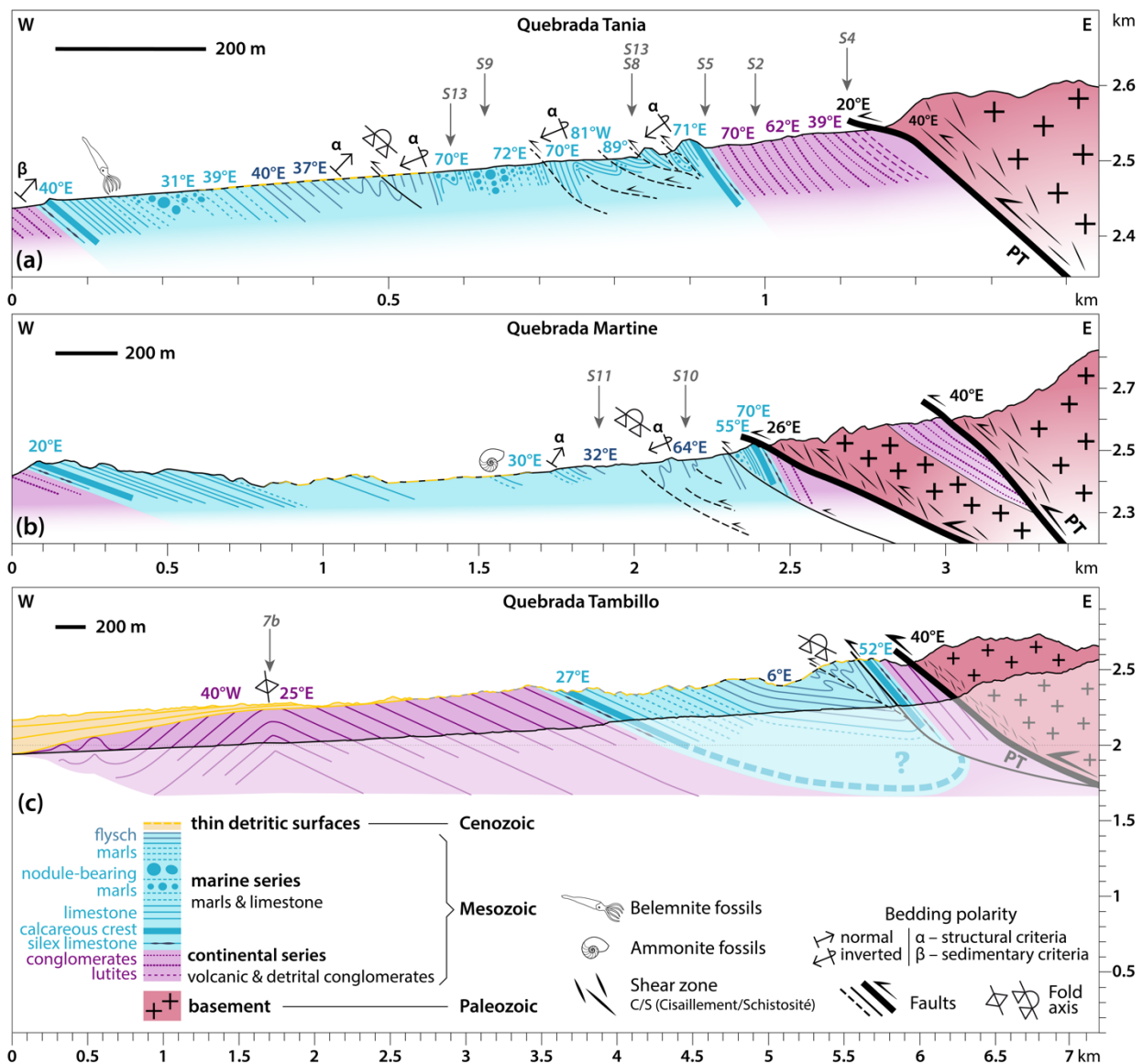
Figure 5. Surface cross-sections along (a) Quebrada Tania, (b) Quebrada Martine, and (c) Quebrada Tambillo (sections A-A', B-B' and C-C' on Figure 4, respectively) . Reported dip angles have been measured in the field or deduced from 3D-mapping. Faults are outlined in black, and dashed when they are only observable at a local spatial scale. Only larger faults (continuous lines) are mapped on Figure 4. Fold axes are depicted above their surface trace, based on our field observations, and their orientation illustrates the deduced orientation of the corresponding axial plane. Grey numbers with arrows point out to field pictures and indicate the associated figure. In the case of Quebrada Tania (a), the sedimentary polarity criterion (β) indicated to the west of the section has been observed ~1 km further downstream than reported here. For Quebrada Martine (b), note the stripe of continental Mesozoic rocks trapped in between two strands of the Pinchal Thrust. Sub-surface interpretation from surface observations is reported with transparent colors in the case of Quebrada Tambillo (c). Note the different spatial scales of the three sections. PT: Pinchal Thrust.

Mesozoic series in the form of numerous local small folds, kinematically indicative of an inverted fold limb (used here as a structural polarity criterium) (Figure S13a), and local secondary shear zones and thrusts (Figure S13b).
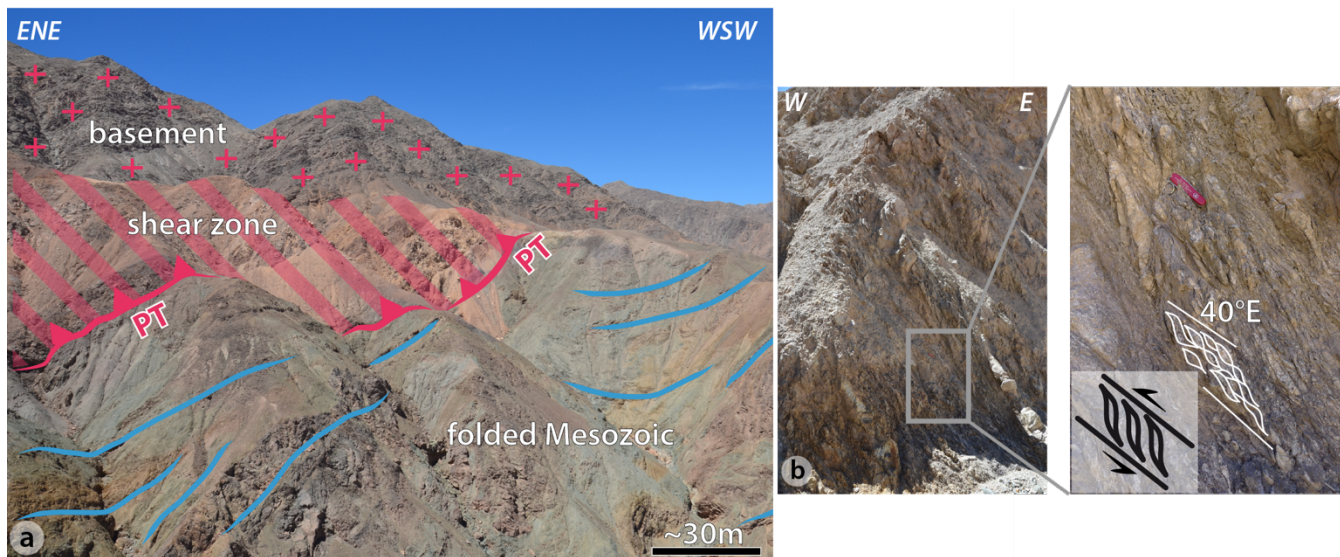
Figure 6. Field characteristics of the Pinchal Thrust.
(a) Field view of the Pinchal Thrust (PT), with dark-grayish Paleozoic basement thrusting over the greenish folded Mesozoic units. Reddish rocks on the hanging wall to the east-northeast correspond to the thrust shear zone (hatched area in picture). Location on Figure 4, note that the scale is here only approximative. Non-interpreted photograph can be found in the supporting information (Figure S15).
(b) Shear band with characteristic C/S-fabric (for "Cisaillement/Schistosité") indicative of top-to-the-west thrusting. Observation within the shear zone in the hanging wall of the Pinchal Thrust (deformed metamorphic basement).

Going westward, as observed in detail along Quebrada Tania (Figure 5a), the eastern part of the black flysch bears small-scale folds characteristic of an inverted fold limb, whereas normal limb folds (used here also as structural polarity criteria) are observed slightly further west: the axis of the overturned west-vergent syncline therefore passes through the black flysch. Part of the Mesozoic series is missing, as overthrusting within the flysch and (marly) limestones is observed frequently along Quebrada Tania (Figure 5a). The overturned syncline is therefore broken by a secondary thrust fault striking approximately parallel to the Pinchal Thrust and roughly coinciding with the synclinal fold axis (Figures 4-5). Westward, the normal western limb of the syncline encompasses the whole Mesozoic series from the black flysch down-section to the Mesozoic volcano-detrital series, with more gentle dip angles (20–40ºE) (Figures 2 and 5). Penetrative deformation is observed to be limited here. The continental Mesozoic layers of the normal limb of the syncline flatten toward the west. The section along Quebrada Tambillo (Figure 5c) shows a broad, overall symmetrical, anticlinal fold (Figure 7b). Its axial plane is steep, dipping ~80°E. Smaller, secondary folds with westward decreasing wavelength and amplitude are found at the western front of this large anticline. Field logistics did not permit further detailed structural observations.

The folded Mesozoic units are unconformably covered by sheet-like, river-incised Cenozoic fluvial deposits, forming aggradational terraces deposited above erosional surfaces at different elevations, of varying spatial extent and of probably different ages (Figure 2). The majority of these erosional surfaces show a westward tilt (Figure 5c). Further west, the Cenozoic deposits become thicker and bury the westward extent of the folded Mesozoic units. Westward thickening of the Cenozoic
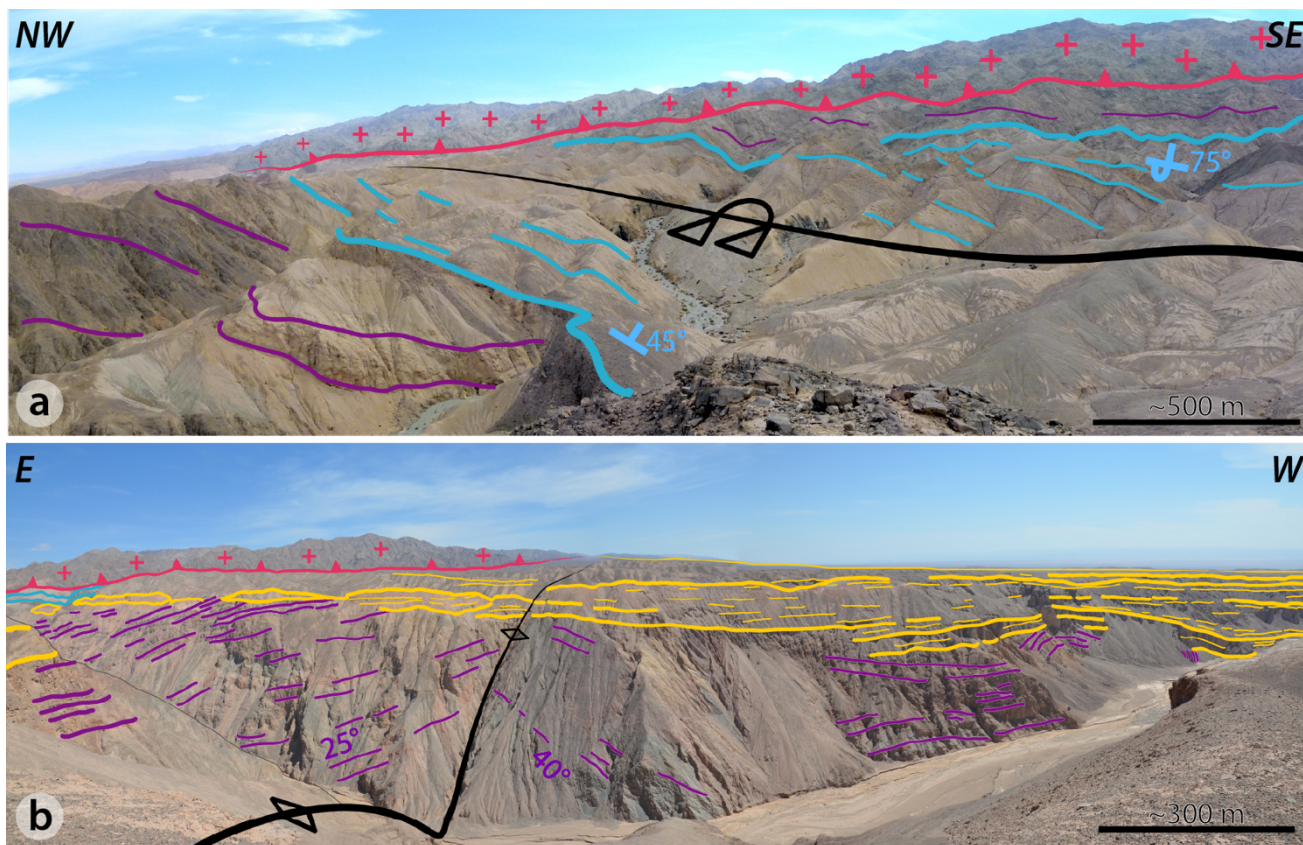
Figure 7. Field pictures of the two major folds within the Pinchal area (location on Figure 4). Non-interpreted photos can be found in the supporting information (Figures S16). Scales are only approximative because of perspective.

(a) Panoramic view over the north-eastern part of the Pinchal area. The Paleozoic basement (red crosses) overthrusts the Mesozoic units (blue and purple horizons) along the Pinchal Thrust (red line with triangles). The topographic low locates the synclinal axis. The calcareous crest on both sides is highlighted by the thick blue lines.

(b) Panoramic view along Quebrada Tambillo, in the southern part of the Pinchal area. The ~200 m deep incised canyon reveals the geometry of the large western anticline affecting Mesozoic layers (purple) underneath the unconformable Cenozoic strata (yellow). The fold axis (black line) probably coincides with an approximately vertical fault, well observable on satellite imagery. Note also the repetition of smaller folds with westward decreasing amplitude and wavelength discernable beneath the westward thickening Cenozoic growth strata to the right of the picture. The Mesozoic calcareous crest (blue) and the Paleozoic basement (red crosses) over the Pinchal Thrust (red) appear in the far eastern background.

layers is observed along Quebrada Tambillo and indicates growth strata at the front of the western anticline (Figures 5c and 7b).

4.3 Comparison to previous stratigraphic and structural interpretations

In the Pinchal area, a basement thrust was reported in the 1:250,000 Quillagua geological map (Skarmeta and Marinovic, 1981). In this map, the Mesozoic units are interpreted as pertaining to the Jurassic Quinchamale formation, deposited in a backarc basin context and composed of an Oxfordian (~157–163 Ma) and a younger Kimmeridgian (~152–157 Ma) sub-unit. Based on this age interpretation and relying on a regionally established Mesozoic stratigraphy where marine sequences are

followed upward by younger clastic deposits, Skarmeta and Marinovic (1981) interpreted the main structure of the Pinchal zone as an anticline.

Our field investigations confirm the existence of a basement thrust, but contradict the earlier interpretation of the folded Mesozoic series and of the local Mesozoic stratigraphy. Even though we do not know the absolute ages of the folded sedimentary series, our structural and sedimentary field observations allow for clearly constraining the relative stratigraphic ages of the folded Mesozoic units, from either structural or sedimentary polarity criteria, and unambiguously indicate that detrital continental units are here stratigraphically below a marine sequence (Figure 3). In the case that the marine strata are Jurassic in age from their likely fossiliferous content, the older continental clastic units could be Triassic, by comparison to recent observations not far from the Pinchal area (Aguilef et al., 2019).

Given this, even though the Pinchal stratigraphic sequence may look in contradiction with the regionally known stratigraphy, it may rather be viewed as complementary: the detrital component observed below marine series may be older than the Jurassic and Cretaceous marine-to-continental upward succession that has been well described regionally. In this sense, the Pinchal area may provide a key outcrop to refine our knowledge of older series, possibly Triassic.

Detailed field pictures of the various stratigraphic and sedimentological observations are provided in supplementary material for reference. In any case, we recall that relative ages are only needed here for the scope of this study to decipher the general structure and deformation pattern.

5 Structure of the folded Mesozoic series at the Quebrada Blanca (~20°45'S)

5.1 Stratigraphy of the Quebrada Blanca area

The stratigraphy at ~20°45'S is well described in the Guatacondo geological map (Blanco and Tomlinson, 2013). Unlike in Pinchal, basement rocks do not crop out in the investigated zone (Figure 8), but larger scale maps (e.g. Sernageomin, 2003) show Paleozoic basement units further east and higher in the topography (Figure 1).

The Mesozoic units of the Quebrada Blanca are of Jurassic to Cretaceous age (Blanco and Tomlinson, 2013). They have been deposited in a back-arc basin context in successive transgression–regression sequences (Charrier et al., 2007), and are subdivided into three formations: (1) The Late Oxfordian Majala Formation, a clastic unit of sandstones, shales and stromatolitic limestones of transitional marine origin; (2) the Late Jurassic / Early Cretaceous Chacarilla Formation, a fluvial clastic sequence; and (3) the Late Cretaceous Cerro Empexa Formation, an andesitic volcanic and continental sedimentary unit (Blanco and Tomlinson, 2013; Blanco et al., 2000; Blanco et al., 2012; Dingman and Galli, 1965; Dingman and Galli Olivier, 1962; Tomlinson et al., 2001). The Majala and Chacarilla Formations both bear detritic reddish and beige sediments. The Cerro Empexa Formation appears greyish and massive in the field. In the Quebrada Blanca area, uranium-lead (U/Pb) dated zircons from this formation bear ages between ~75 and ~68 Ma (Blanco and Tomlinson, 2013; Blanco et al., 2012; Tomlinson et al., 2015) (Figure 8).
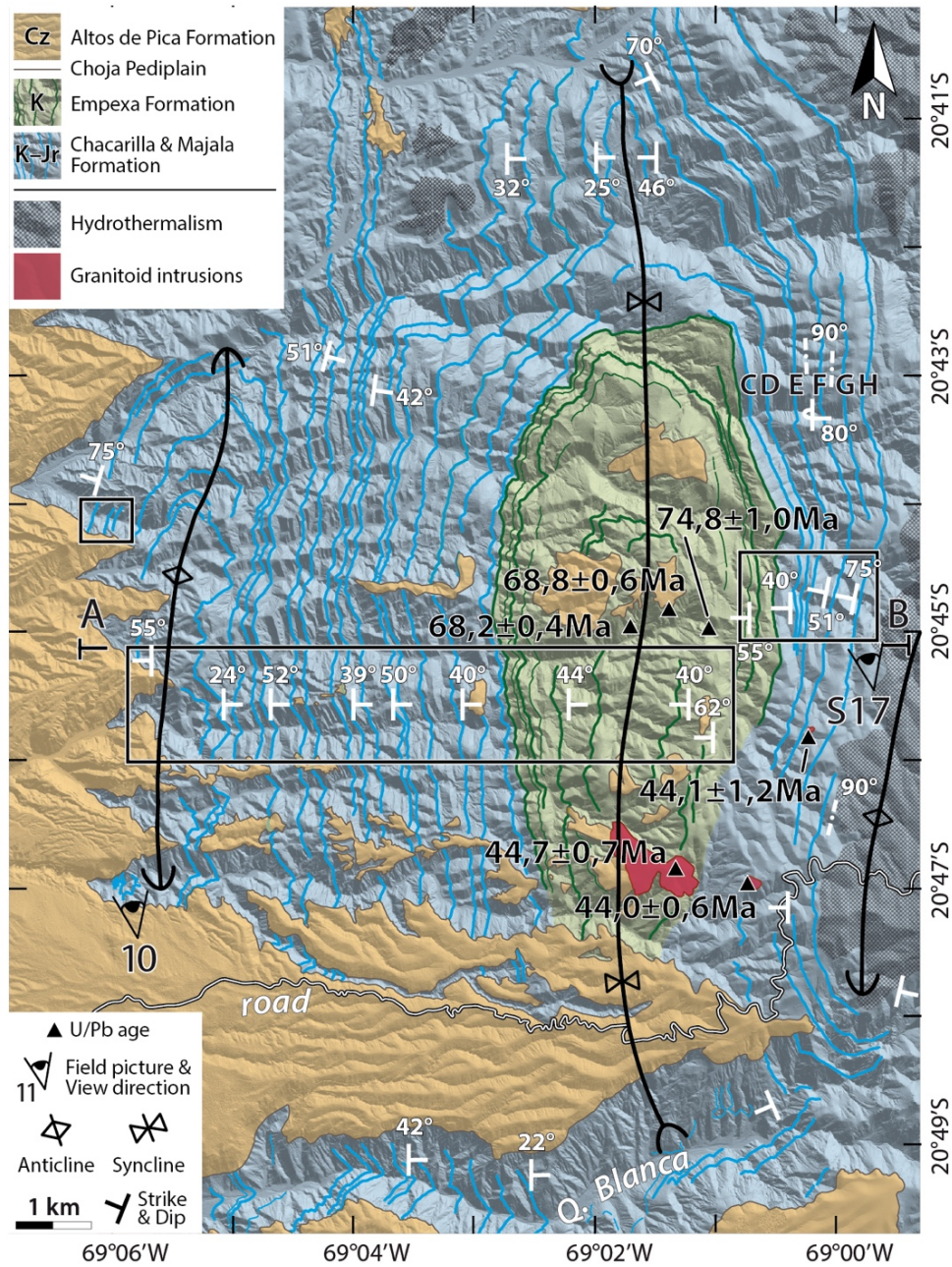
Figure 8. Structural map of the Quebrada Blanca zone, refined from Armijo et al. (2015) (location on Figure 1). Colored lines report mappable layers. For visibility, only major, well-correlated layer traces are represented here. Black boxes locate where mapped layers were considered and projected for the construction of the structural east–west surface cross-section (Figure 9). The A–B section corresponds to the topographic profile used for this cross-section. Strike and dip measurements are extracted from 3D-mapping (see section 3.3) or observed in the field. Strike symbols without dip value are derived from satellite imagery. Field pictures are located (with view direction), and numbered according to the associated figure. Ages from uranium-lead (U/Pb) radioisotope dating on zircon are taken from the Guatacondo geological map (Blanco and Tomlinson, 2013). Letters C, D, E, F, G and H to the north-east (within the folded Chacarilla and Majala Formations) report the layers illustrated on Figure S17 in supplementary material. Background hillshaded DEM produced from tri-stereo Pléiades imagery. Cz: Cenozoic; K: Cretaceous; Jr: Jurassic; Q: Quebrada.
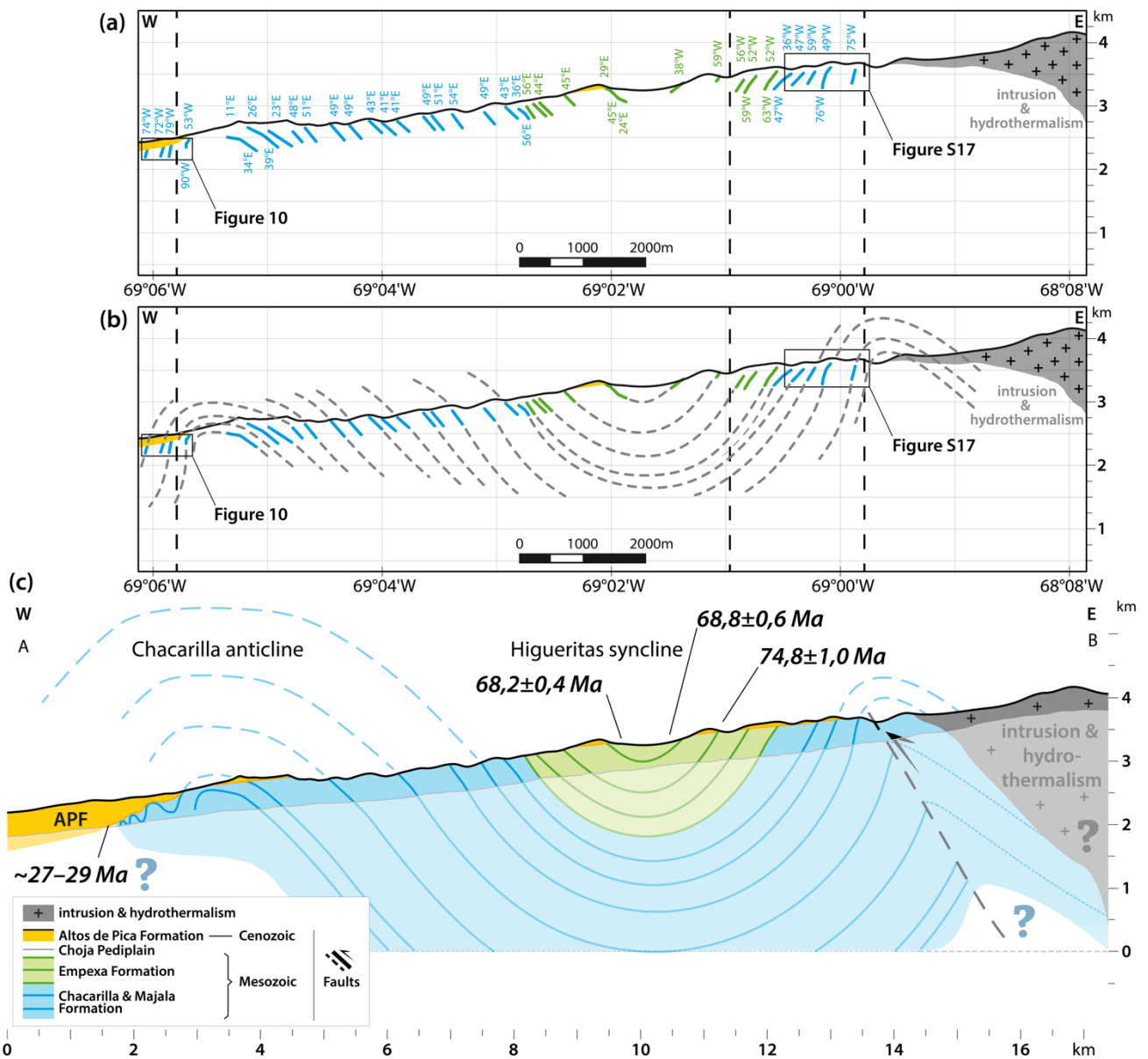
Figure 9. East–west surface cross-section of the Quebrada Blanca site, established from the projection of selected, well-expressed layers mapped on satellite imagery. APF: Altos de Pica Formation.

(a) Observations, reporting the geometry of projected layers and associated dip angles, together with their stratigraphic ages (color-code).

(b) Sub-surface interpretation and extrapolation of observations.

(c) East–west sub-surface section A-B based on (a) and (b). Interpretation at depth is indicated with transparent colors, in contrast with surface observations. Extrapolation above the topographic surface is drawn with dashed lines. Ages from uranium-lead (U/Pb) radioisotope dating on zircon are taken from the Guatacondo geological map (Blanco and Tomlinson, 2013). The ~27–29 Ma age of the basal deposits of the Altos de Pica formation is derived from regional considerations (Victor et al., 2004).

445

450

Magmatic intrusions and hydrothermalism occur locally, and hide the eastern continuation of the folded Mesozoic series. Some of these intrusions are dated by uranium-lead (U/Pb) on zircons at ~44 Ma (Blanco and Tomlinson, 2013) (Figure 8).

The Cenozoic deposits of the Altos de Pica Formation here also overlie the Mesozoic series, over the Choja Pediplain angular unconformity (see also section 2.2). The age of the basal deposits of the Altos de Pica Formation is regionally estimated to
455 ~27–29 Ma (e.g. Victor et al., 2004).

5.2 Structural observations

Although the cartography of the folds is complicated by the blanketing Cenozoic cover (notably in the west and south), and by magmatic intrusions and hydrothermalism (particularly to the east) (Figure 8), three large-scale folds are observable: a wide syncline in the center (Higueritas syncline), bounded by two anticlines to the west (Chacarilla anticline) and east (fold names
460 from Blanco and Tomlinson, 2013; Fuentes et al., 2018). The scale of these folds is multi-kilometric (Figure 8). Both anticlines are asymmetric: they have steeper western limbs (dip angles vary between ~50–80ºW), whereas their eastern limbs have more gentle dip angles (varying between ~20–50ºW) (Figure 9). Despite the fact that the eastern flank of the eastern anticline is widely hidden by magmatic intrusions and hydrothermalism, its southern part is well observable in the field (Figure 8). The central Higueritas syncline is wider and more symmetric, with dip angles of ~40–50° on both limbs. The anticlines involve the
465 Majala and Chacarilla Formations, while the core of the syncline bears the Cerro Empexa Formation. Overall, the documented folds show a clear west-vergence (Figure 9c).

In the field, we observe small-scale deformation within both anticlines (Figure 9). A series of anticlines with westward decreasing amplitude and wavelength (of a few tens to a few hundreds of meters – to be compared to the ~4 km wavelength of the main anticline) are observable on the western edge of the Chacarilla anticline (Figures 9c and 10). In the field, at least
470 one of these small-scale folds is affected by a minor thrust. Additionally, within the eastern large-scale anticline, a thrust-affected small-scale fold is observed (Figures 9c and S17), and confirms the west-vergence at this smaller scale.

The Cenozoic detrital units are unconformably deposited above the folded Mesozoic series. Thin sheet-like river-incised Cenozoic surfaces remain in the central part, becoming more dominant to the South and West (Figure 8). These superficial erosional surfaces show an overall westward tilt (Figure 9). Westward thickening of the Cenozoic layers deposited above the
475 erosional Choja surface is clearly observed at the front of the western anticline (Figure 10) and reveals the presence of growth strata.

6 Kinematics of shortening of the Pinchal and Quebrada Blanca areas

6.1 Timing of deformation

The projection of mapped strata indicates that the Mesozoic series is overall concordant in Quebrada Blanca (Figure 9). The
480 cross-section of the Guatacondo map (Blanco and Tomlinson, 2013) suggests however the presence of a minor angular unconformity (<10º) at the base of the Cerro Empexa formation, not observed here from our large-scale high-resolution
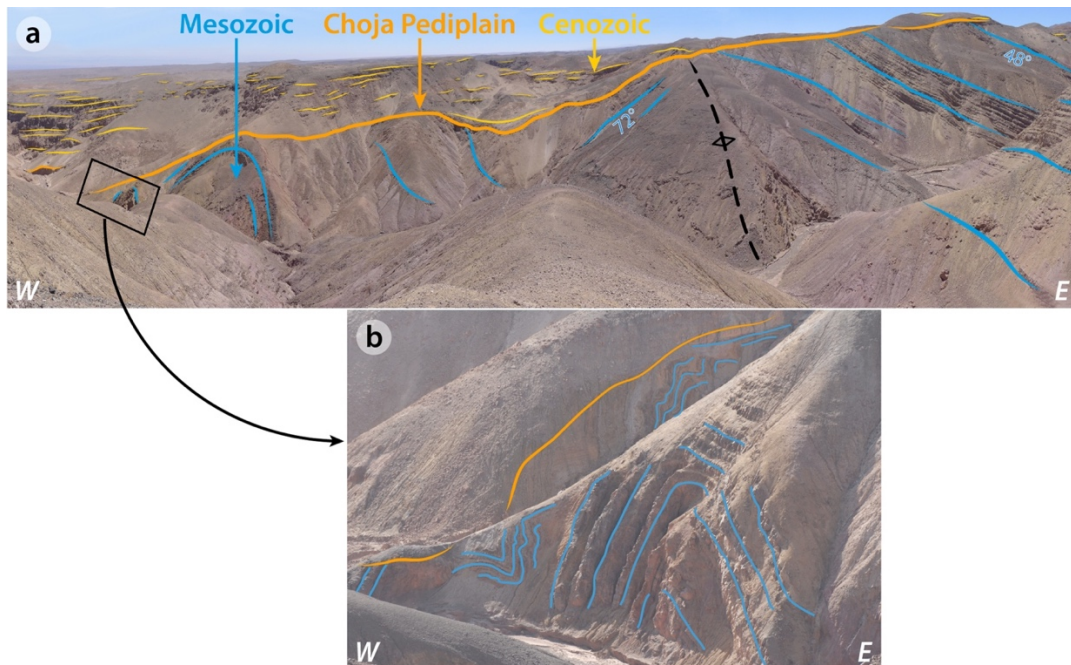
Figure 10. Field picture of the western limb of the western anticline in the Quebrada Blanca area. Non-interpreted photographs are provided in supplementary material (Figure S18). Location on Figures 8 and 9.

485 (a) Series of folds with westward decreasing amplitude and wavelength (hundreds to tens of meters) observed at the front of the western anticline.

(b) Detailed view of the westernmost outcropping small-scale anticlines, located on (a) by the black box.

mapping. As this local unconformity does not produce any major change in the geometry of layers from Jurassic to Cretaceous,

490 we consider it to be minor, in particular with respect to the main large-scale folding documented here. Folding therefore mostly post-dates the deposition of all these series. In the Quebrada Blanca area, the youngest folded layers of the Cerro Empexa Formation bear U-Pb ages of 68.9±0.6 Ma and 68±0.4 Ma (Blanco and Tomlinson, 2013) (Figures 8 and 9c). We can therefore conclude that the main deformation episode post-dates ~68 Ma, even though we cannot exclude earlier but minor deformation when compared to the observed large-scale folding (Figure 9c).

495 Magmatic intrusions dated at ~44 Ma intrude the folded Mesozoic units, and appear cartographically not affected by folding (Blanco and Tomlinson, 2013) (Figure 8). This suggests that the major part of the folding occurred during the ~68–44 Ma time interval. However, without additional observations of the deformation – or not – of these intrusions (geometry of the contact with surrounding host units, mineral deformation…), we cannot unequivocally conclude here from this simple cartographic observation.

500 Even though we suspect that the deformed series of the Pinchal zone are Triassic to Jurassic, we do not have any absolute ages of the folded units. Therefore, we postulate that the main deformation here also post-dates ~68 Ma by analogy to our observations at the Quebrada Blanca.

The folded Mesozoic units are unconformably covered by the Cenozoic Altos de Pica Formation at both investigated sites. This is also the case for the Pinchal Thrust and secondary thrusts at few places in the Pinchal zone (Figure 4). The presence of

505 growth strata at the front of the westernmost anticlines in both study areas, over the erosional Choja Pediplain, suggests that some deformation proceeded after ~29 Ma, during deposition of the Altos de Pica Formation. However, the deformation recorded by folded Mesozoic units appears of greater intensity than that of the Cenozoic growth layers (Figures 5c and 9c). Given this, we propose that the main folding of the Mesozoic layers documented here can be bracketed to a maximum time span of ~40 Myr, sometime between ~68 Ma and ~29 Ma, with additional relatively minor deformation after ~29 Ma. Possibly,

510 the main deformation period could be shorter (~24 Myr at most), sometime between ~68 Ma and ~44 Ma, with minor shortening after the Eocene intrusions. In the case of the Pinchal Thrust, we can only propose from our observations that thrusting took place prior to ~29 Ma.

6.2 Structural Interpretations

6.2.1 Section across the Pinchal zone

515 The cross-section proposed along Quebrada Tambillo (Figures 11b-c) summarizes our preferred interpretation of the sub-surface structural geometry of the Pinchal area.

Considering that the folds west of the Pinchal Thrust develop above underlying thrusts is a reasonable and classical assumption (Davis et al., 1983; Suppe, 1983). These thrusts have dip angles parallel to the layers forming the backlimb of the overlying anticlines (as proposed in Figures 11b-c), or can be steeper. They are expected to root at least at the base of the outcropping

520 folded Mesozoic series (as proposed in Figures 11b-c), or deeper. From there, it can be extrapolated that the thrusts root at least 2 km beneath the topographic surface (i.e. at ~0.2 km a.s.l.), assuming that the layer thickness is constant over our study area. We cannot discard the possibility that the thrusts root deeper and are steeper from surface geology alone. To the west of our field area, at the front of the anticline, the small-scale folds with westward decreasing wavelength and amplitude (Figure 7b) are interpreted as the possible expression of disharmonic folding within the forelimb of the anticline and/or of a thrust

525 ramping-up toward the sub-surface (Figures 11b-c).

Using the simplified geometry of layers along Quebrada Tambillo (Figures 5c and 11c), line-length balancing results in a minimum of ~1 km of shortening absorbed by folding only, from the Pinchal Thrust to the front of the anticline (Table 1). Because of the pervasive presence of small-scale folding and thrusting (Figures 5a-b and S13), in particular within the inverted limb of the overthrusted syncline, this estimate represents a minimum value. A significant – but unconstrained – amount of

530 shortening by folding is surely to be added. In addition to folding, the offsets on the interpreted underlying thrusts are to be considered when quantifying shortening. However, the thrust offsets largely depend on the interpreted thrust geometry and on the structure of the footwall, which can not be precisely determined from surface geology.

Based on the dip angle of the C/S-fabric of the shear-zone (Figure 6b) and on the mapping of the thrust on satellite imagery, we estimate that the Pinchal Thrust dips ~40ºE in the near-surface, locally less such as along Quebradas Tania and Martine

535   (Figures 5a-b). All secondary strands of the Pinchal Thrust are expected to root at depth onto the main shear-zone. The secondary thrust breaking the core of the syncline, roughly parallel to the Pinchal Thrust (Figure 4), may be described as an out-of-the-syncline thrust (Mitra, 2002) and probably also connects onto it at depth. A similar reasoning is proposed to all small-scale thrusts and décollements observed within the inverted synclinal limb. The minimum thickness of the Mesozoic series is estimated to ~2.2 km from the normal limb of the syncline along Quebrada Tambillo. Thus, it can be considered that

540   the strict minimum exhumation of the basement is equally of ~2.2 km. Assuming a constant 40°E dip angle and taking exhumation as a proxy for structural uplift, this yields a minimum displacement of ~2.6 km on the Pinchal thrust only.

6.2.2 Section across the Quebrada Blanca

As for the Pinchal area, we interpret the Quebrada Blanca folds as related to ramp thrusts rooting at least at the base of the folded Mesozoic units - ie at the base of the Late Jurassic series - , or deeper. Assuming constant layer thicknesses, it can be

545   deduced that the thrusts root at least 4 km beneath the current topographic surface (i.e. at least at –2 km a.s.l.) (Figure 11a). In our cross-section of Figure 11a, the interpreted thrust needs to deepen eastward to balance the proposed section. From surface geology alone, we cannot discard the possibility that the thrust is steeper below the documented anticlines and roots deeper. The secondary frontal folds with westward decreasing wavelength (Figures 10 and 11a) can be explained as disharmonic folds within the forelimb of the large western anticline and/or be interpreted as reflecting the existence of a shallow blind thrust

550   (Figure 11a). Such a feature is also in good agreement with secondary (steeper) thrusts affecting these anticlines (Figure 9). Line-length-balancing of the cross-section of Figure 11a results in ~3.8 km of shortening solely related to folding (Table 1). This value is only a minimum as it does not account neither for the observed small-scale deformation nor for slip on the related thrusts at depth. As for Pinchal, the fault geometries and the structure of the footwall of the thrusts are not constrained from surface geology to provide a complete cross-section and the associated shortening.

555 **6.3 Additional constraints on shortening: a possible structural interpretation modeled by trishear**

The underlying thrusts have not reached the surface and remain blind (Figures 5c and 9c). They are also associated with disharmonic folding at their probable tip, with small-scale folds at the front of major anticlines. Because of these observations, we assume fault-propagation-folding to be the dominant mode of deformation in both study areas. To estimate the amount of shortening that is taken by thrusting at depth, some assumptions on the footwall and thrust geometries are needed.

560   One possible interpretation is to consider a thrust ramp parallel to the layers of the backlimb of the anticlines, rooting at the base of the series involved in folding, as in the sections of Figure 11. Disharmonic folding at the front of the anticlines is likely related to the local thickening of layers at the front of a shallow upward propagating ramp, as in the frontal triangular zone of trishear folds. To further quantify the shortening associated to this chosen structural interpretation, we do kinematic trishear modeling (e.g. Allmendinger, 1998; Erslev, 1991) of the westernmost anticlines documented at the Quebrada Tambillo

565   (Pinchal area) and Quebrada Blanca. This approach accounts for folding, slip on propagating thrust-faults, and models the
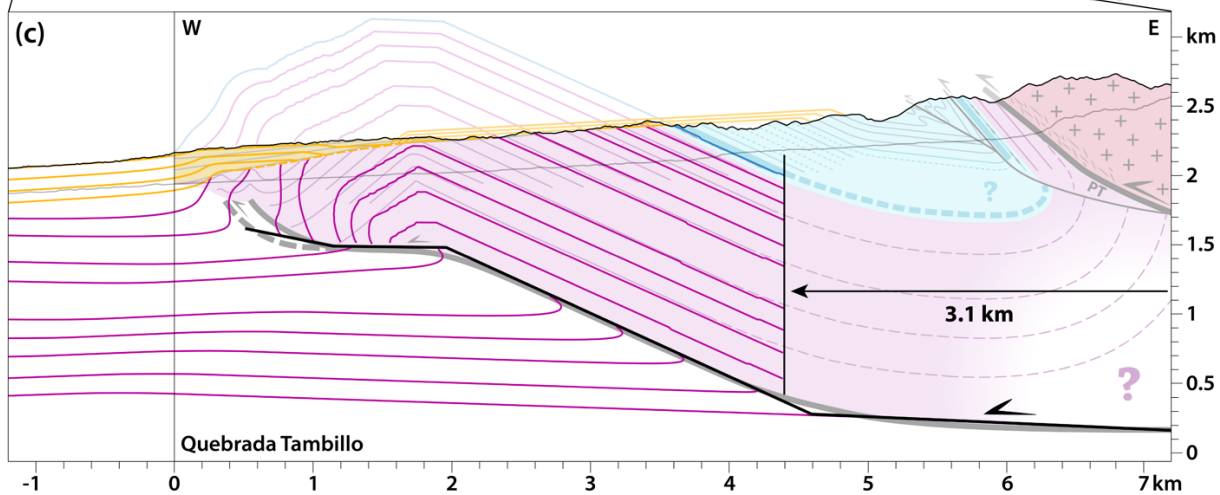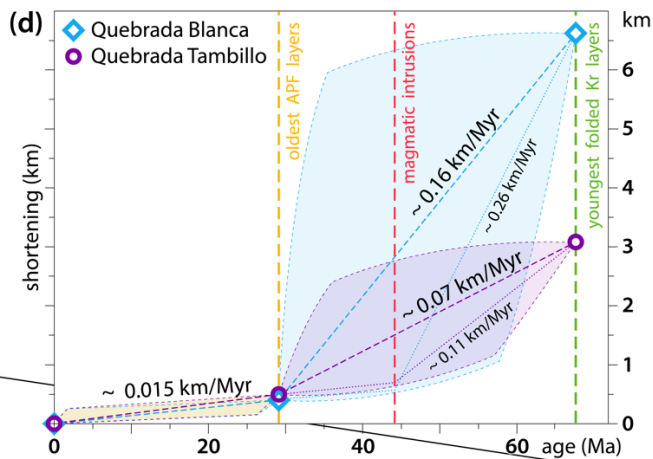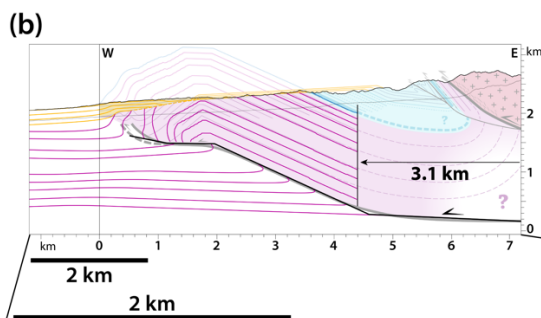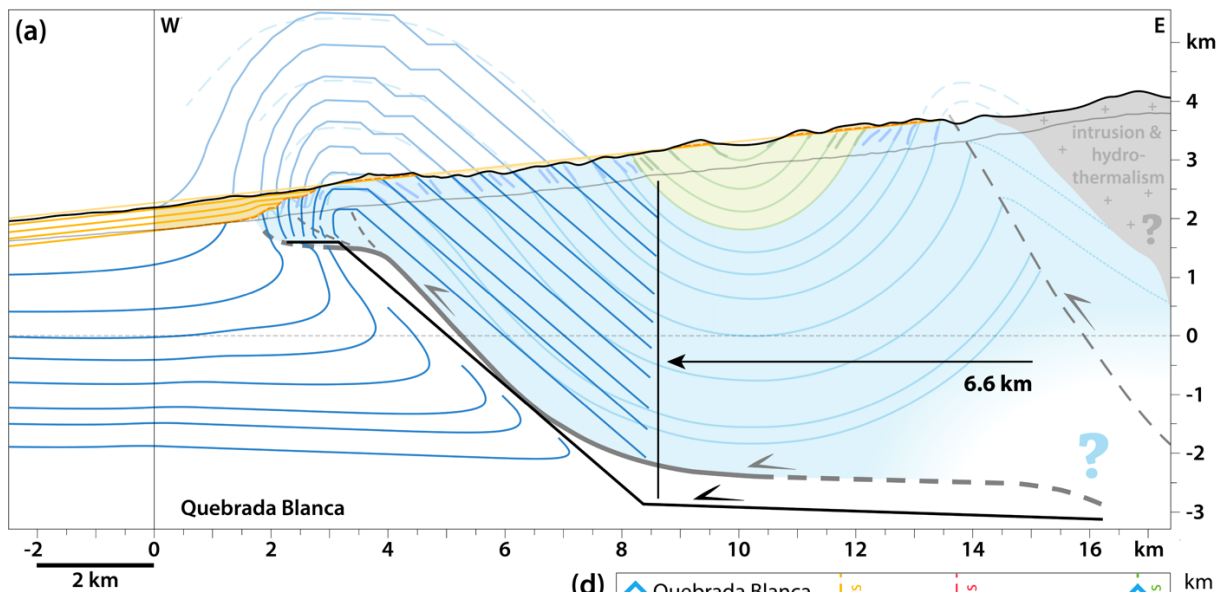
Figure 11 (previous page). Cross-sections and kinematics of folding of the Quebrada Blanca and Pinchal zones. Cross-sections are built from field observations considering that faults root at the base of the folded series. Modeling was performed with FaultFold Forward v.6 (Allmendinger, 1998). Intermediate stages of the trishear modeling are reported on Figures S19 and S20 for the cross-sections of Quebrada Tambillo and Quebrada Blanca, respectively. Model parameters are reported in Tables S2–S3.

(a-c) Proposed cross-sections and final stages of our preferred trishear models in the case of (a) the Quebrada Blanca area; (b) the Quebrada Tambillo (Pinchal area) shown here at the same scale as (a). (c) Detailed and enlarged view of our results for the Quebrada Tambillo. Note the large scale-difference between the sections of the two investigated sites (a,b). Thicker lines outline model results, while transparent lines and colors refer to the proposed cross-sections. Black lines report the modeled thrusts and horizontal arrows report the modeled total shortening. PT: Pinchal Thrust.

(d) Shortening vs. time, as deduced from trishear modeling of the western anticlines of the Quebrada Blanca and Pinchal areas, and the ages of deformed layers. The three temporal benchmarks correspond to the age of the youngest folded Cretaceous (Kr) unit (~68 Ma), to the age of magmatic intrusions possibly post-dating folding (~44 Ma), both derived from the Guatacondo geological map (Blanco and Tomlinson, 2013), and to the ~29 Ma age of the oldest Cenozoic layer of the Altos de Pica Formation (APF) (Victor et al., 2004). It is possible that most deformation occurred prior to ~44 Ma (steeper lines). Our results underline two phases of deformation, with a slowing down of deformation since ~29 Ma at least, possibly even before.

	Pinchal	Quebrada Blanca
Folding (*line-length balancing*)	West anticline: ~0.6 km East anticline: > 0.4 km Total: > 1 km	West anticline: 1.8 km East anticline+syncline: 2 km Total: 3.8 km
Folding + thrusting (*trishear modeling*)	West anticline: 3.1 km	West anticline: 6.6 km
Basement thrusting (*structural section*)	Pinchal Thrust : >2.6 km	-
Total	Folds (folding + thrusting): > 3.5 km Total (folds + PT): > 6.1 km	Folds (folding + thrusting): > 8.6 km

Table 1: Shortening values on the various structures documented in this study. Shortening associated to folding is estimated from line-length balancing on the various folds of the two investigated sites. Additional constraints on shortening are provided for the western anticlines from trishear modeling; these include folding of these anticlines and thrusting on the associated ramp. Thrusting on the Pinchal Thrust (PT) is deduced from its sub-surface geometry and the minimum thickness of the folded Mesozoic series. See text for additional details.

deformation distributed at the tip of these evolving faults. The trishear formalism relies on a set of parameters that are adjusted here by trial and error, so as to visually fit the proposed structural geometries of the anticlines. The values of these parameters are within the range considered in previous studies (Tables S1-S3) (e.g. Allmendinger, 1998; Allmendinger and Shaw, 2000; Cristallini and Allmendinger, 2002; Erslev, 1991; Hardy and Ford, 1997; Zehnder and Allmendinger, 2000), and 65-100 combinations of these parameters have been tested here. Further details are provided in supplementary material (Text S1).

Here we present our preferred models, which allow for reproducing satisfactorily the proposed structural geometries, acknowledging that these solutions are not unique. The structural geometries of the westernmost anticlines of the two study sites are reproduced (Figure 11), and the evolution of deformation is modeled over time taking into account the Cenozoic growth strata. The various stages of deformation are shown in Figures S19 and S20 in the supplementary material. We find

that the geometries of the western anticlines can be reproduced with a cumulative shortening of 3.1 km for Quebrada Tambillo (Pinchal area), and of 6.6 km for Quebrada Blanca (Figure 11). Based on the range of tested acceptable models, we estimate that these shortening values are determined here with an uncertainty of ~0.2 km.

The above shortening values only account for the deformation (folding and thrusting) absorbed across the modeled westernmost anticlines. Synclinal folding accounts for an additional minimum shortening of ~0.4 km as deduced by line-length-balancing in the Pinchal area, leading to a total of >3.5 km of shortening across the Mesozoic units along the Quebrada Tambillo section. This includes folding, as well as slip on the detachment and western thrust ramp (Table 1). When adding the minimum ~2.6 km of thrusting deduced on the Pinchal Thrust, we get >6.1 km of total shortening across the whole Pinchal area. Similarly, in the Quebrada Blanca area, the easternmost anticline and syncline take up ~2 km of shortening by folding deduced by line-length-balancing, leading to a minimum amount of shortening of ~8.6 km across the whole Quebrada Blanca section, including folding and slip on the underlying detachment and western ramp (Table 1).

The two investigated sites take up different amounts of shortening. This may relate to the fact that the across-strike extent of the two sections are significantly different (~7 km long section for the Quebrada Tambillo vs. ~17 km long section for the Quebrada Blanca) (Figure 11). The calculated shortenings similarly represent ~47% and ~34% of shortening when scaled to the extent of the Quebradas Tambillo and Blanca sections, respectively. Differences between these sections may also relate to the depth at which the interpreted thrusts root (elevation of ~0.2 km for Quebrada Tambillo vs. depth of ~2 km for Quebrada Blanca, relative to sea level) (Figure 11), which is a probable result of the varying structural and stratigraphic inheritance from the earlier Andean basins. Lateral variations in deformation can also not be excluded.

The shortening values estimated above depend on the proposed sub-surface structural interpretations, and more specifically on the thrust geometries - much more than on the detailed model parameters. They are to be considered lower bounds, but only within the considered structural framework. We favored the simplest geometry where the thrusts root at the base of the folded series and connect at depth, but cannot discard from local field observations alone the possibility that they are steeper and root deeper. If this were the case, shortening related to thrusting would be lower than proposed here. Folding estimated from line-length balancing only and our favored structural interpretation (Figure 11) therefore provide a lower and upper bound on shortening estimates, respectively.

6.4 Kinematics of shortening

Within the structural framework proposed in the sections of Figure 11, trishear modeling allows for simulating the evolution of thrust slip and folding in the case of the westernmost anticlines of the two investigated sites. By adding syntectonic layers while deformation proceeds, we also reproduce the overall geometry of the base of the Cenozoic Altos de Pica Formation deposits and of the subsequent growth strata (Figures S19 and S20). Syntectonic surfaces and layers are prescribed an initial 3–6° W dipping angle, similar to the present-day regional topographic slope (Figure 1). From there, we find that ~0.5 km and ~0.4 km of shortening are needed to reproduce the first-order geometry of the base of the Altos de Pica Formation at the front of the Quebrada Tambillo (Pinchal area) and Quebrada Blanca sections, respectively, using the previous trishear models

adjusted to our final cross-sections. When compared to the minimum 3.1 km and 6.6 km of total shortening accumulated since ~68 Ma across the westernmost anticlines of these two sections, this indicates that the ~29 Ma old basal Cenozoic layers above the Choja surface record at most only 16% and 6% of this total shortening, respectively. We have tested the possibility of initial horizontal Cenozoic syntectonic layers. In this case, a post- ~29 Ma shortening of 0.8 km at most is needed to best adjust the observed geometry of the basal Altos de Pica Formation layers, even though a good fit to both the geometry of the growth strata and of the finite fold structure cannot be satisfactorily found.

These results are then used to quantitatively describe the evolution of shortening over time across the westernmost anticlines of the two interpreted sections, with account on the timing of deformation discussed in section 6.1 (Figure 11d). We find that shortening rates were on average of ~0.07–0.16 km/Myr over the time span ~68–29 Ma. They could have been even as high as ~0.11–0.26 km/Myr if considering that the main deformation phase is confined to ~68–44 Ma. Subsequently, deformation rates decreased to an average value of ~0.015 km/Myr after ~29 Ma, starting possibly earlier.

These average values are most probably minimum values, within the framework of our modeled structural interpretations. Indeed, thrusting and folding are here only modeled for the westernmost anticlines of our study sites, and do not account for the shortening cumulated neither across the other structures nor on the Pinchal Thrust. Also, the main phase of deformation prior to ~29 Ma could have lasted less than the ~68–29 Ma or ~68–44 Ma considered time intervals, respectively (Figure 11d). In the case that the underlying faults are steeper and root deeper, these minimum values would be both similarly lower.

Our results therefore quantitatively emphasize our former qualitative conclusion that the major phase of deformation occurred sometime between ~68 and ~29 Ma, with a significant subsequent slowing down of deformation rates afterwards, possibly as soon as ~44 Ma or earlier (Figure 11d), a general conclusion that is not dependent on the proposed sub-surface thrust geometries.

7 Discussion

7.1 The Andean Basement Thrust

7.1.1 Evidencing a major basement thrust system along the West Andean flank (~20–22°S)

Here, we have further documented the Pinchal Thrust, which brings basement units of the Sierra de Moreno westward over folded Mesozoic units. Our study in the Pinchal area suggests that this thrust bears local complexities with several strands and minor splays, most probably related to the reactivation of structures in the initial pre-Andean back-arc basins. Laterally, the geological map of Skarmeta and Marinovic (1981) clearly documents this structure from ~21º15'S to 21º35'S, and possibly down to ~22°S with some structural complexities by ~21º35'S with the junction of two possible strands of this basement thrust.
 Similar basement thrusts have been described all along the Cordillera Domeyko between ~20°S and ~22°S. North of the map by Skarmeta and Marinovic (1981), the Quehuita (up to ~21º11'S) and Choja (between ~21º08'S–21º01'S) Faults are west-vergent thrusts bringing basement over folded Mesozoic sediments (Aguilef et al., 2019). North of ~21ºS, intrusions,

hydrothermalism and surface volcanics hamper clear observation of similar basement thrusts. Such basement thrusts, if existent, would however provide a reasonable mechanism for the exhumation and exposure of basement rocks east of the folded Mesozoic units and at higher elevations, at the latitude of Quebrada Blanca (~20°45'S) (Figure 1). For these reasons, we cannot tell with any certainty whether a thrust contact similar to that described in Pinchal (this study) and further north (Aguilef et al., 2019) exists at this latitude, but such structure is to be suspected.

South of the map by Skarmeta and Marinovic (1981), in the Sierra de Moreno at ~21°45'S, Haschke and Gunther (2003)'s section report a basement thrust over folded Mesozoic units, in agreement with the style of deformation documented here, but with a relatively minor displacement compared to our results in Pinchal. This thrust is here called the Sierra de Moreno Thrust. Together with the 1:1,000,000 Geological map of Chile (Sernageomin, 2003), Haschke and Gunther (2003)'s map suggests that this basement thrust is cartographically continuous southward to the southern end of the Sierra de Moreno, at ~22°05'S. This possibly documents its lateral termination.

As a conclusion, there exists a series of west-vergent basement thrusts all along the Western Andean flank, with various strands mapped as local basement faults, as in our study (Figure 4) or in other maps (Aguilef et al., 2019; Haschke and Gunther, 2003; Sernageomin, 2003; Skarmeta and Marinovic, 1981; Tomlinson et al., 2001). Altogether, these thrusts appear as a major structural boundary all along the Western Andean flank, bringing the basement of the Cordillera Domeyko westward over folded Mesozoic units of the earlier Andean basins (Figures 1 and 12)– and therefore contributing to the uplift of the western margin of the Altiplano. They form a segmented thrust system extending laterally over at least ~120 km north-south (Figure 1), that we propose to name here the Andean Basement Thrust (hereafter ABT) system.
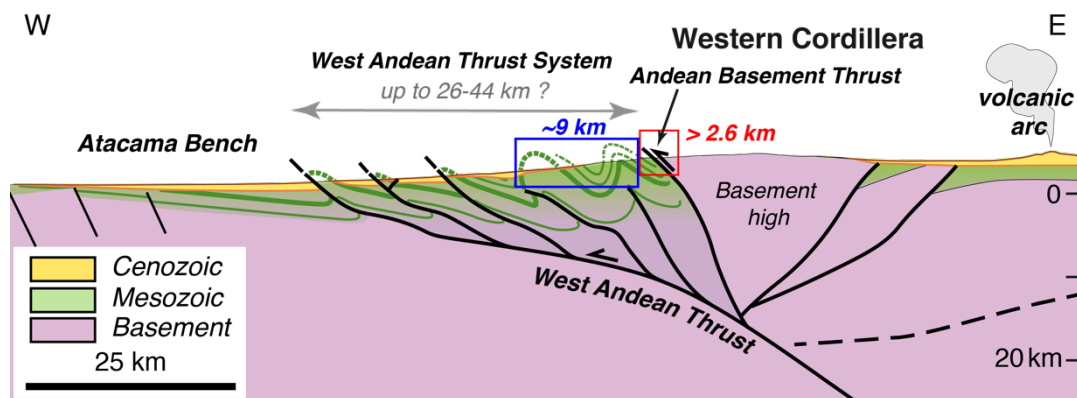
Figure 12: Schematic section across the Western Cordillera (20-22°S), modified after Armijo et al. (2015). This section is only meant to be illustrative of the general structural framework of the Western Andes at the investigated latitudes. Color rectangular frames locate the structures equivalent to the Quebrada Blanca folds (blue) and to the Pinchal Thrust (red) studied here. Shortenings estimated at these sites are reported. Shortening values in grey are tentatively estimated by upscaling our local findings to the whole West Andean Thrust System. The various thrusts need to root at depth onto an east-dipping decollement (West Andean Thrust), whose depth is not constrained. See text for further details.

690 We interpret the ABT to dip eastward beneath the Western Cordillera, at least >2 km (Pinchal area) or >4 km (Quebrada Blanca area) beneath the present-day topographic surface. Deeper and eastward, this thrust probably connects to a crustal-scale ramp, as needed to sustain the large-scale uplift and topographic rise of the Western Andes (Figures 1 and 12), following the earlier ideas by Victor et al. (2004) and Armijo et al. (2015). Such crustal-scale structure has been termed the West Andean Thrust (or WAT) by Armijo et al. (2015).

7.1.2 Shortening and timing of deformation of the Andean Basement Thrust

695 We estimated that the Pinchal Thrust (as part of the ABT system) accommodated a minimum of ~2.6 km of shortening over a horizontal distance of ~1 km in Pinchal. This estimate is deduced from the geometry of the thrust and from the minimum ~2.2 km of exhumation needed to erode Mesozoic series and expose basement at the surface, considering here that exhumation is a proxy for structural uplift. Thermochronological data are too limited to evaluate the amount of basement exhumation more

700 precisely, as well as its timing. These data are presently absent locally in Pinchal, but sparsely exist at the regional scale when considering the ABT system over its whole extent. From apatite fission track dating in basement samples taken ~20 km east and south-east of our two study sites, Maksaev and Zentilli (1999) inferred at least 4–5 km of basement exhumation occurring between ~50–30 Ma. Such exhumation is consistent with our results when considering the exhumation that may have accompanied the uplift expected from overthrusting on the ABT, and on the WAT further east. Older thermochronological

705 ages – (U-Th)/He zircon and apatite ages of ~91 Ma and ~57 Ma, respectively – were found by Reiners et al. (2015) from the basement of the Quebrada Arcas, ~30 km south of Pinchal, in a structural setting equivalent to that documented here. These ages do not contradict the previous estimates on total exhumation by Maksaev and Zentilli (1999), even though modeling would be needed here to precisely test this. However, they question the exact timing of basement exhumation, and, from there, of thrusting over the ABT. In the absence of properly analyzed and modeled samples closer to the ABT, it is difficult to assess

710 more precisely its timing or amount of exhumation, uplift and thrusting.

At a few places, the Pinchal segment of the ABT is covered by Cenozoic deposits. Given this observation and with existing thermochronological ages, we postulate that the ABT was most probably active sometime by Late Cretaceous to Early Cenozoic – and that its activity had ceased by Early Miocene. This suggests it may have been coeval with folding of the Mesozoic units documented immediately further west – or starting slightly before.

7.2 The West Andean Thrust System at ~20–22ºS

7.2.1 Evidencing a west-vergent thrust system along the West Andean flank (~20–22°S)

The west-vergent folds described here as deforming Mesozoic units at ~20–22ºS are interpreted to form above faults. A similar system of folds and faults affecting Mesozoic units is expected to extend further north and south than just the two sites described here, most probably over the entire zone of ~20–22ºS (Figure 1), even though a large part north of Quebrada Blanca

720   is covered by Cenozoic strata. This is deduced from existing maps and previous works (e.g. Aguilef et al., 2019; Haschke and Gunther, 2003; Sernageomin, 2003; Skarmeta and Marinovic, 1981). It therefore probably spreads out over a north-south distance of at least ~200 km – and possibly more as folded Mesozoic sediments are mapped on the 1:1,000,000 Geological map of Chile (Sernageomin, 2003) in the north- and south-ward continuation of the two zones investigated here.

    Further west, structures at depth are hidden beneath Cenozoic deposits (Figure 1). Seismic profiles from the Chilean Empresa

725   Nacional del Petroleo (ENAP), as re-interpreted by various authors (Victor et al., 2004; Fuentes et al., 2018; Labbé et al., 2019; Martinez et al., 2021), show also a series of several blind mostly west-vergent thrust faults. The faults and folds documented here across two ~7–17 km wide sites therefore most probably pertain to a thrust system that extends across-strike over a much wider region (~50 km, maybe locally more).

    West-verging thrust faults along the Western Andes at ~20-22°S most probably derive from the inversion of the normal faults

730   that bounded the earlier Andean basins. Fuentes et al. (2018) and Martinez et al. (2021) interpreted these faults as single planar deep-reaching thrusts, possibly rooting into basement. However, even though such geometries cannot be discarded from local poorly resolved seismic data or from scarse field observations, they cannot satisfactorily explain the large-scale geometry of the Western Andean flank, as noted earlier by Victor et al. (2004). Indeed, only a ramp-flat-ramp geometry of a basal master fault deeping eastward beneath the Western Cordillera, whatever its rooting depth, can account for the overall large-scale

735   continuous topographic rise of the entire western plateau margin (Figures 1 and 12) (Armijo et al., 2015; Victor et al., 2004). The blind west-vergent thrust-faults found all along the western flank at ~20–22°S can therefore reasonably be interpreted as connecting onto such an east-dipping master fault (or detachment). By integrating our local observations into these regional large-scale considerations, we favor the earlier interpretations of Victor et al. (2004) and Armijo et al. (2015).

    Altogether, these data suggest that all these thrust faults, either hidden below Cenozoic deposits or deduced from outcropping

740   folds, most possibly pertain to a common west-vergent thrust system, found all along the Western Cordillera of North Chile (20-22°S). We propose to name this thrust system the West Andean Thrust System (or WATS). The WATS at ~20–22°S therefore extends laterally over at least ~200 km, and across-strike over a much wider region (~50 km, maybe locally more) than the two ~7–17 km wide sites investigated in this study (Figures 1 and 12).

7.2.2 Shortening across the West Andean Thrust System (~20-22°S)

745   By excluding the possibility of steep deep-rooting single faults from the above large-scale considerations, we favor our local structural interpretations of Figure 11 - and from there the associated shortening estimates - where the faults possibly root at the base of the folded series, at least locally. The WATS of northern Chile (~20–22°S) therefore probably accommodates a minimum shortening of ~3–9 km, as quantified from the ~7–17 km wide investigated areas (not including the contribution of the ABT in Pinchal). At ~21°45'S, ~30 km south of the Pinchal area, Haschke and Gunther (2003) report a minimum shortening

750   of >9 km from a ~50 km wide cross-section in the Sierra de Moreno area and further east. Within the ~8–10 km wide area encompassing an equivalent of the WATS and ABT, they estimate a minimum shortening of ~4 km (i.e. a minimum of ~30% of shortening), a value consistent and at scale with our results. This study of Haschke and Gunther (2003) is to our knowledge

the only other work attempting to estimate the minimum total shortening absorbed by the WATS. It becomes obvious that the various structures of the WATS in northern Chile, wherever they are (Quebrada Blanca, Pinchal or Sierra Moreno areas), all absorb multi-kilometric shortening, at the scale of only one to three major folds and thrusts.

This conclusion further emphasizes that the ~3–9 km of shortening proposed here from the folds of the Quebrada Blanca and Pinchal areas (when excluding the contribution of the ABT in Pinchal) are in any case under-estimates of the total shortening across the whole WATS. When applying the minimum ~34–47% shortening estimated across our two investigated sites to the ~50 km across-strike extent of the whole WATS, we tentatively propose a possible crustal shortening of ~26–44 km (Figure 12), a value consistent – even though in the high range – with the ~20–30 km qualitatively estimated by Armijo et al. (2015) by scaling with structural relief and crustal thickness. These estimates should however be taken with caution and only as possible upper bounds, as deformation is localized on thrust faults (e.g. Fuentes et al., 2018; Haschke and Gunther, 2003; Martinez et al., 2021; Victor et al., 2004; this study) and not homogeneously distributed. Also the precise geometry of faults at depth, in particular their rooting depth, is in no case constrained. A precise quantification of the deformation recorded by buried folded Mesozoic units west of our study sites is at the moment not possible from available seismic profiles.

7.3 Temporal evolution of deformation along the Western Andes (~20–22°S)

Our investigations underline that the deformation of the Quebrada Blanca and Pinchal areas is not linearly distributed over time, and can be assigned to two main periods: (1) a period of major deformation sometime between ~68–29 Ma (possibly ~68–44 Ma); and (2) a subsequent period of moderate deformation from ~29–0 Ma (starting possibly earlier) (Figure 11d). This is deduced for the westernmost anticline of both study sites from trishear modeling, but the reduction in deformation rates is expected at the scale of the whole investigated sites as the difference in the deformation cumulated by Mesozoic units and by post ~29 Ma Cenozoic layers can be qualitatively – but clearly – intuited from our field observations and cross-sections (Figures 5, 9 and 11). Westward, deformation is mostly well-imaged on seismic profiles for Cenozoic post- ~29 Ma growth strata and remains less well-resolved for underlying Mesozoic units (Fuentes et al., 2018; Labbé et al., 2019; Martinez et al., 2021; Victor et al., 2004), reflecting the fact that Mesozoic units could here also be much more deformed than Cenozoic layers. In this study, we find ~0.4–0.5 km of post ~29 Ma shortening on one single most frontal fault and fold in the case of our two investigated sections (Figures S19, S20), that is over a distance of ~5–8 km. Based on the ENAP seismic profiles in the westward prolongation of our study areas, Victor et al. (2004) determined a post ~29 Ma shortening of ~3 km, accommodated by several west-vergent thrusts within the ~40 km wide Atacama Bench. All these values are in overall good agreement when setting them to the same spatial scale, as they consistently represent ~6–8% of shortening. Compared to the minimum ~3–6 km of ante- ~29 Ma shortening (or ~34–47% of shortening) quantified on one single structure in this study (Figures S19, S20), the post ~29 Ma shortening is clearly of limited importance.

The deformation slow-down, starting by ~29 Ma at latest and possibly earlier by ~44 Ma, could therefore be regional across the entire WATS. This reasoning applies to the WATS but may also hold for the ABT. If the age of basement thrusting is not

785 precisely known, it most probably occurred by Early Cenozoic (Maksaev and Zentilli, 1999) or even Late Cretaceous - Early Cenozoic (deduced after Reiners et al. (2015)), and had ceased by ~29 Ma (see discussion in section 7.1).

This proposed time window for major folding and possibly for thrusting over the ABT is generally consistent with the main Incaic phase of deformation inferred by various authors as the main period of Andean mountain-building *stricto sensu* (e.g. Charrier et al., 2007; Cornejo et al., 2003; Pardo-Casas and Molnar, 1987; Steinmann, 1930). The simplest interpretation on

790 the post ~29 Ma decline of the shortening rate is that it results from the slow-down of the same protracted regional compressional event which caused the formation of the west-vergent WATS and ABT. With the presently available data at 20–22°S, we cannot exclude that this slow-down may have started before ~29 Ma – possibly as soon as ~44 Ma, or even before (section 6.4) – but definitely not afterwards.

7.4 Regional implications

795 Even though multi-kilometric, the shortening accommodated by the west-vergent structures of the Western Andes outlined in this study represents a modest contribution to the total crustal shortening of >300 km across the entire Central Andes at ~20ºS (e.g. Anderson et al., 2017; Barnes and Ehlers, 2009; Eichelberger et al., 2013; Elger et al., 2005; Kley and Monaldi, 1998; Mcquarrie et al., 2005; Sheffels, 1990). It should however be recalled that the deformation absorbed across the Western Andes took place mostly in the early stages of the Andean orogeny, sometime between ~68–29 Ma (possibly ~68–44 Ma) in the case

800 of the WATS, starting possibly earlier for the ABT – in any case during the Incaic phase. In fact, when replaced within the temporal evolution of Andean mountain-building at these latitudes (e.g. Armijo et al., 2015; Charrier et al., 2007; Mcquarrie et al., 2005; Oncken et al., 2006) (see section 2.1), the early multi-kilometric shortening evidenced here represents a major contribution to initial Andean deformation, which has been most often neglected in orogen-wide studies. The slowing down of deformation across the Western Andean flank by ~29 Ma – and possibly starting after ~44 Ma – may have accompanied the

805 jumping and transfer of deformation towards the East, i.e. towards the eastern Altiplano and further east (e.g. Isacks, 1988; Mcquarrie et al., 2005; Oncken et al., 2006).

8 Conclusion

In this study, we investigate and explore from two outcropping sites two major structural features within the western flank of the Chilean Andes at ~20–22°S: (1) the Andean Basement Thrust (ABT) system, which stands as a system of west-vergent

810 thrusts bringing Paleozoic basement over folded Mesozoic series; (2) the West Andean Thrust System (WATS), which is a west-vergent thrust system deforming Mesozoic and Cenozoic sediments. The WATS is mostly hidden by the Cenozoic Altos de Pica Formation, but structures crop out in few (up to ~10–20 km wide) places along the mountain flank. Even though our investigations only rely on two limited outcropping sites, our deductions have regional implications when compared and up-scaled with previous results.

Using field and satellite observations, we build structural cross-sections and quantify the recorded shortening at two key sites along the western mountain flank. We estimated a minimum shortening of >2.6 km on the ABT and of >3–9 km on the few exposed structures of the WATS. This shortening – derived from outcrop areas of limited extent – corresponds only to a fraction of the entire deformation at the scale of the whole Western Cordillera at ~20–22ºS. When set on scale with the extent of the investigated structures, it implies the possibility of multi-kilometric shortening across the western flank of the Andes, possibly up to 26–44 km.

We further exploit the differential deformation recorded by folded Mesozoic layers and Cenozoic growth strata of the post ~29 Ma Altos de Pica Formation. We show that the outcropping WATS was mainly active between ~68–29 Ma (possibly ~68–44 Ma), and that its deformation rates significantly decreased after ~29 Ma (a decrease that may have started earlier, e.g. by ~44 Ma). By comparison to previous studies of the blind portions of the WATS west of our study sites, we propose that such slowing-down of deformation rates was regional rather than local. In addition, field observations and published thermochronological results of basement exhumation suggest that this temporal evolution of deformation rates may also hold for the ABT. We therefore propose that the post ~29 Ma (or post ~44 Ma) decline in shortening rates resulted from the regional slowing-down of the same protracted compressional event that caused the formation of the west-vergent WATS and ABT, most probably accompanying the transfer of Andean deformation towards the Altiplano Plateau, Eastern Cordillera, and further eastward.

Data availability

Pleiades satellite imagery (https://earth.esa.int/eogateway/missions/pleiades) was obtained through the ISIS program of the CNES under an academic license, and is not available for open distribution. On request, the DEMs calculated from this imagery can be provided to any academic researcher, however after approval from the CNES (contact: isis-pleiades@cnes.fr, with copy to lacassin@ipgp.fr and simoes@ipgp.fr, and referring to this manuscript). Numerical computations for the DEMs were performed using the free and open source MicMac software suite (Rosu et al., 2014; Rupnik et al., 2016) freely available at https://micmac.ensg.eu/index.php. For cartographic mapping, we also used Google Earth imagery (Landsat 7, DigitalGlobe) freely accessible at https://earth.google.com. All geological maps used in this work are cited in the main text and in the reference section. Our own maps are provided in the main text. All field measurements and observations have been collected by us during our field missions (march 2018, january 2019) and are provided in the main text, in the figures and in the supporting information. The trishear kinematic modeling was conducted using FoldFault Forward version 6 (Allmendinger, 1998), freely available at http://www.geo.cornell.edu/geology/faculty/RWA/programs/faultfoldforward.html

Supplementary Data

Author contribution

845 RL and MS designed the study and TH carried it out. TH designed all figures. The manuscript was prepared by TH, MS and RL, and revised by MS and RL - with the contribution of all co-authors. All authors participated to field work and to the various scientific discussions.

Competing interests

The authors declare that they have no conflict of interest.

Acknowledgements

850 This study was supported by grants from CNRS-INSU (program TELLUS-SYSTER) and from the Institut de physique du globe de Paris (IPGP) (PI: RL). Field work was also funded by the Andean Tectonics Laboratory of the Advanced Mining Technology Center, University of Chile (PI: DC). Earlier work on this zone by RL and DC was supported by ANR project MegaChile (grant ANR-12-BS06-0004-02) and LABEX UnivEarthS project. TH benefited from a PhD grant attributed by the 855 French Ministry of Higher Education and Research. Pleiades satellite imagery was obtained through the ISIS program of the CNES under an academic license. The authors thank A. Delorme for his technical assistance in producing the DEMs, using the free and open-source MicMac software. Numerical computations for the DEMs were performed on the S-CAPAD platform, Institut de physique du globe de Paris (IPGP). The kinematic modeling was made using FoldFault Forward version 6. R. Armijo and the late R. Thiele are warmly thanked for the fruitful discussions that led over the years to this work and manuscript. 860 We also benefited from discussions with C. Creixell, N. Blanco, A. Tomlinson and F. Sepulveda (SERNAGEOMIN), from the valuable help of M. Riesner for the 3D mapping, and that of L. Barrier for facies and polarity identifications. L. Barrier and N. Bellhasen are also thanked for inspiring discussions. Comments by L. Giambiagi, C. Mpodozis and R. Allmendinger on an earlier version of this manuscript are acknowledged. Constructive reviews by B. Gérard and P. Baby helped improve this manuscript. This study was partly supported by IdEx Université de Paris ANR-18-IDEX-0001.

865

References

Aguilef, S., Franco, C., Tomlinson, A., Blanco, N., Álvarez, J., Montecino, D., Gardeweg, M., Campos, V., Rodríguez, C., and Maksaev, V.: Geología Del Área Quehuita-Chela, Regiones De Tarapacá Y Antofagasta, 1: 100.000, 2019.

Allmendinger, R. W.: Inverse and forward numerical modeling of trishear fault-propagation folds, Tectonics, 17, 640-656, 10.1029/98TC01907, 1998.

Allmendinger, R. W. and Shaw, J. H.: Estimation of fault propagation distance from fold shape: Implications for earthquake hazard assessment, Geology, 28, 1099-1102, 10.1130/0091-7613(2000)28<1099:EOFPDF>2.0.CO;2, 2000.

Anderson, R. B., Long, S. P., Horton, B. K., Calle, A. Z., and Ramirez, V.: Shortening and structural architecture of the Andean fold-thrust belt of southern Bolivia (21 S): Implications for kinematic development and crustal thickening of the central Andes, Geosphere, 13, 538-558, 10.1130/GES01433.1, 2017.

Armijo, R., Lacassin, R., Coudurier-Curveur, A., and Carrizo, D.: Coupled tectonic evolution of Andean orogeny and global climate., Earth-Science Reviews, 143, 1-35, 2015.

Armijo, R., Rauld, R., Thiele, R., Vargas, G., Campos, J., Lacassin, R., and Kausel, E.: The West Andean thrust, the San Ramon Fault, and the seismic hazard for Santiago, Chile., Tectonics, 29, 10.1029/2008TC002427, 2010.

Baker, M.: Geochronology of Upper Tertiary volcanic activity in the Andes of North Chile, Geologische Rundschau, 66, 455-465, 10.1007/BF01989588, 1977.

Barnes, J. B. and Ehlers, T. A.: End member models for Andean Plateau uplift. , Earth-Science Reviews, 97, 105-132, 10.1016/j.earscirev.2009.08.003, 2009.

Blanco, N. and Tomlinson, A.: Carta Guatacondo, Región de Tarapacá, Servicio Nacional de Geología y Minería, Carta Geológica de Chile, Serie Geología Básica, 2013.

Blanco, N., Tomlinson, A. J., Moreno, K., and Rubilar, D.: Importancia estratigráfica de las icnitas de dinosaurios presentes en la Formación Chacarilla (Jurásico-Cretácico Inferior), Región de Tarapacá, Chile, 9e Congreso geológico chileno,

Blanco, N., Vásquez, P., Sepúlveda, F., Tomlinson, A., Quezada, A., and Ladino, M.: Levantamiento geológico para el fomento de la exploración de recursos minerales e hídricos de la Cordillera de la Costa, Depresión Central y Precordillera de la Región de Tarapacá (20-21 S), Servicio Nacional de Geología y Minería, Santiago, Chile, 2012.

Brooks, B. A., Bevis, M., Whipple, K., Ramon Arrowsmith, J., Foster, J., Zapata, T., Kendrick, E., Minaya, E., Echalar, A., and Blanco, M.: Orogenic-wedge deformation and potential for great earthquakes in the central Andean backarc, Nature Geoscience, 4, 380-383, 10.1038/ngeo1143, 2011.

Buchelt, M. and Cancino, C. T.: The Jurassic La Negra Formation in the area of Antofagasta, northern Chile (lithology, petrography, geochemistry), in: The Southern Central Andes, edited by: Bahlburg, H., Breitkreuz, C., and Giese, P., Lecture Notes in Earth Sciences, Springer, Berlin, 169-182, 10.1007/BFb0045181, 1988.

Charrier, R., Pinto, L., and Rodríguez, M. P.: Tectonostratigraphic evolution of the Andean orogen in Chile., The Geology of Chile, 21-114, 2007.

Cornejo, P., Matthews, S., and Perez, C.: The « K-T » compresive deformation event in northern Chile (24°-27°S). 10th Congreso Geologico Chileno, Concepcion, Chile,

Cristallini, E. O. and Allmendinger, R. W.: Backlimb trishear: a kinematic model for curved folds developed over angular fault bends, Journal of Structural Geology, 24, 289-295, 10.1016/S0191-8141(01)00063-3, 2002.

Davis, D., Suppe, J., and Dahlen, F.: Mechanics of fold-and-thrust belts and accretionary wedges, Journal of Geophysical Research: Solid Earth, 88, 1153-1172, 1983.

905 DeCelles, P., Zandt, G., Beck, S., Currie, C., Ducea, M., Kapp, P., Gehrels, G., Carrapa, B., Quade, J., and Schoenbohm, L.: Cyclical orogenic processes in the Cenozoic central Andes, Geological Society of America Memoirs, 212, MWR212-222, 10.1130/2015.1212(22), 2014.

DeMets, C., Gordon, R. G., Argus, D. F., and Stein, S.: Effect of recent revisions to the geomagnetic reversal time scale on estimates of current plate motions, Geophysical research letters, 21, 2191-2194, 10.1029/94GL02118, 1994.

910 Dingman, R. J. and Galli, O. C.: Geology and ground-water resources of the Pica area, Tarapaca Province, Chile, Geological Survey Bulletin, 1188-1189, US Department of Interior1965.

Dingman, R. J. and Galli Olivier, C.: Cuadrángulos Pica, Alca, Matilla y Chacarilla, con un estudio sobre los recursos de agua subterránea: Provincia de Tarapacá. Escala 1: 50.000, Instituto de Investigaciones Geologicas, Carta Geologica de Chile, 1962.

Eichelberger, N., McQuarrie, N., Ehlers, T. A., Enkelmann, E., Barnes, J. B., and Lease, R. O.: New constraints on the
915 chronology, magnitude, and distribution of deformation within the central Andean orocline, Tectonics, 32, 1432-1453, 10.1002/tect.20073, 2013.

Elger, K., Oncken, O., and Glodny, J.: Plateau-style accumulation of deformation: Southern Altiplano, Tectonics, 24, 10.1029/2004TC001675, 2005.

Erslev, E. A.: Trishear fault-propagation folding, Geology, 19, 617-620, 10.1130/0091-
920 7613(1991)019<0617:TFPF>2.3.CO;2, 1991.

Faccenna, C., Oncken, O., Holt, A. F., and Becker, T. W.: Initiation of the Andean orogeny by lower mantle subduction., Earth and Planetary Science Letters, 463, 189-201, 2017.

Farías, M., Charrier, R., Comte, D., Martinod, J., and Hérail, G.: Late Cenozoic deformation and uplift of the western flank of the Altiplano: Evidence from the depositional, tectonic, and geomorphologic evolution and shallow seismic activity (northern
925 Chile at 19 30′ S), Tectonics, 24, 10.1029/2004TC001667, 2005.

Fuentes, G., Martínez, F., Bascuñan, S., Arriagada, C., and Muñoz, R.: Tectonic architecture of the Tarapacá Basin in the northern Central Andes: New constraints from field and 2D seismic data, Geosphere, 14, 2430-2446, 10.1130/GES01697.1, 2018.

Galli-Olivier, C.: Pediplain in northern Chile and the Andean uplift, Science, 158, 653-655, 10.1126/science.158.3801.653,
930 1967.

Garcia, M. and Hérail, G.: Fault-related folding, drainage network evolution and valley incision during the Neogene in the Andean Precordillera of Northern Chile, Geomorphology, 65, 279-300, 10.1016/j.geomorph.2004.09.007, 2005.

Garzione, C. N., McQuarrie, N., Perez, N. D., Ehlers, T. A., Beck, S. L., Kar, N., Eichelberger, N., Chapman, A. D., Ward, K. M., and Ducea, M. N.: Tectonic evolution of the Central Andean plateau and implications for the growth of plateaus, Annual
935 Review of Earth and Planetary Sciences, 45, 529-559, 10.1146/annurev-earth-063016-020612, 2017.

Hardy, S. and Ford, M.: Numerical modeling of trishear fault propagation folding, Tectonics, 16, 841-854, 10.1029/97TC01171, 1997.

Haschke, M. and Gunther, A.: Balancing crustal thickening in arcs by tectonic vs. magmatic means, Geology, 31, 933-936, 10.1130/G19945.1, 2003.

940 Heit, B., Sodoudi, F., Yuan, X., Bianchi, M., and Kind, R.: An S receiver function analysis of the lithospheric structure in South America, Geophysical Research Letters, 34, 10.1029/2007GL030317, 2007.

Henriquez, S., DeCelles, P. G., and Carrapa, B.: Cretaceous to middle Cenozoic exhumation history of the Cordillera de Domeyko and Salar de Atacama basin, northern Chile, Tectonics, 38, 395-416, 10.1029/2018TC005203, 2019.

Homewood, P. and Lateltin, O.: Classic swiss clastics (flysch and molasse) The alpine connection, Geodinamica Acta, 2, 1-945 11, 10.1080/09853111.1988.11105150, 1988.

Horton, B. K.: Sedimentary record of Andean mountain building, Earth-Science Reviews, 178, 279-309, 10.1016/j.earscirev.2017.11.025, 2018.

Isacks, B. L.: Uplift of the central Andean plateau and bending of the Bolivian orocline, Journal of Geophysical Research: Solid Earth, 93, 3211-3231, 10.1029/JB093iB04p03211, 1988.

950 Jaillard, E., Hérail, G., Monfret, T., Diaz-Martinez, E., Baby, P., Lavenu, A., and Dumont, J. F.: Tectonic evolution of the Andes of Ecuador, Peru, Bolivia and northern Chile, in: Tectonic evolution of South America, edited by: Cordani, U. G., Milani, E. J., Thomaz Filho, A., and Campos, D. A., Rio de Janeiro, Brazil, 481-559, 2000.

Kley, J. and Monaldi, C. R.: Tectonic shortening and crustal thickness in the Central Andes: How good is the correlation?, Geology, 26, 723-726, 10.1130/0091-7613(1998)026<0723:TSACTI>2.3.CO;2, 1998.

955 Labbé, N., García, M., Simicic, Y., Contreras-Reyes, E., Charrier, R., De Pascale, G., and Arriagada, C.: Sediment fill geometry and structural control of the Pampa del Tamarugal basin, northern Chile, GSA Bulletin, 131, 155-174, 10.1130/B31722.1, 2019.

Lamb, S.: Did shortening in thick crust cause rapid Late Cenozoic uplift in the northern Bolivian Andes?, Journal of the Geological Society, 168, 1079-1092, 10.1144/0016-76492011-008, 2011.

960 Lamb, S.: Cenozoic uplift of the Central Andes in northern Chile and Bolivia—reconciling paleoaltimetry with the geological evolution, Canadian Journal of Earth Sciences, 53, 1227-1245, 10.1139/cjes-2015-0071, 2016.

Lucassen, F., Becchio, R., Wilke, H., Franz, G., Thirlwall, M., Viramonte, J., and Wemmer, K.: Proterozoic–Paleozoic development of the basement of the Central Andes (18–26° S)—a mobile belt of the South American craton, Journal of South American Earth Sciences, 13, 697-715, 10.1016/S0895-9811(00)00057-2, 2000.

965 Maksaev, V. and Zentilli, M.: Fission track thermochronology of the Domeyko Cordillera, Northern Chile: implications for Andean tectonics and porphyry copper metallogenesis., Exploration and Mining Geology, 8, 65-89, 1999.

Martinez, F., Fuentes, G., Perroud, S., and Bascuñan, S.: Buried thrust belt front of the western Central Andes of northern Chile: Style, age, and relationship with basement heterogeneities, Journal of Structural Geology, 147, 104337, 10.1016/j.jsg.2021.10433, 2021.

970 McQuarrie, N.: The kinematic history of the central Andean fold-thrust belt, Bolivia: Implications for building a high plateau, Geological Society of America Bulletin, 114, 950-963, 10.1130/0016- 7606(2002)114<0950:TKHOTC>2.0.CO;2, 2002.

McQuarrie, N., Horton, B. K., Zandt, G., Beck, S., and DeCelles, P. G.: Lithospheric evolution of the Andean fold–thrust belt, Bolivia, and the origin of the central Andean plateau, Tectonophysics, 399, 15-37, 10.1016/j.tecto.2004.12.013, 2005.

Mitra, S.: Structural models of faulted detachment folds, AAPG bulletin, 86, 1673-1694, 10.1306/61EEDD3C-173E-11D7-
975 8645000102C1865D, 2002.

Mpodozis, C., Ramos, V., Ericksen, G., Cañas Pinochet, M., and Reinemund, J.: The Andes of Chile and Argentina, in: Geology of the Andes and its Relation to Hydrocarbon and Mineral Resources, edited by: Ericksen, G. E., Canas Pinochet, M. T., and Reinemund, J. A., Earth Sciences Series, Circum-Pacific Council for Energy and Mineral Resources Houston, Texas, 59-90, 1989.

980 Muñoz, N. and Charrier, R.: Uplift of the western border of the Altiplano on a west-vergent thrust system, northern Chile, Journal of South American Earth Sciences, 9, 171-181, 10.1016/0895-9811(96)00004-1, 1996.

Norabuena, E., Leffler-Griffin, L., Mao, A., Dixon, T., Stein, S., Sacks, I. S., Ocola, L., and Ellis, M.: Space geodetic observations of Nazca-South America convergence across the central Andes, Science, 279, 358-362, 10.1126/science.279.5349.358, 1998.

985 Oncken, O., Hindle, D., Kley, J., Elger, K., Victor, P., and Schemmann, K.: Deformation of the central Andean upper plate system—Facts, fiction, and constraints for plateau models, in: The Andes - Active subduction orogeny, edited by: Oncken, O., Chong, G., Franz, G., Giese, P., Götze, H.-J., Ramos, V. A., Strecker, M. R., and Wigger, P., Frontiers in Earth Sciences, Springer, Berlin, Germany, 3-27, 10.1007/978-3-540-48684-8_1, 2006.

Pardo-Casas, F. and Molnar, P.: Relative motion of the Nazca (Farallon) and South American plates since Late Cretaceous
990 time, Tectonics, 6, 233-248, 10.1029/TC006i003p00233, 1987.

Puigdomenech, C., Somoza, R., Tomlinson, A., and Renda, E.: Paleomagnetic data from the Precordillera of northern Chile: A multiphase rotation history related to a multiphase deformational history, Tectonophysics, 791, 228569, 10.1016/j.tecto.2020.228569, 2020.

Ramos, V. A.: Late Proterozoic-early Paleozoic of South America-a collisional history, Episodes Journal of International
995 Geoscience, 11, 168-174, 1988.

Rapela, C., Pankhurst, R. J., Casquet, C., Baldo, E., Saavedra, J., and Galindo, C.: Early evolution of the Proto-Andean margin of South America, Geology, 26, 707-710, 10.1130/0091-7613(1998)026<0707:EEOTPA>2.3.CO;2, 1998.

Reiners, P. W., Thomson, S. N., Vernon, A., Willett, S. D., Zattin, M., Einhorn, J., Gehrels, G., Quade, J., Pearson, D., and Murray, K. E.: Low-temperature thermochronologic trends across the central Andes, 21 S–28 S, in: Geodynamics of a
1000 Cordilleran Orogenic System: The Central Andes of Argentina and Northern Chile, edited by: DeCelles, P. G., Ducea, M. N., Carrapa, B., and Kapp, P. A., Memoir, Geological Society of America, 215-249, 10.1130/2015.1212(12), 2015.

Reutter, K.-J., Scheuber, E., and Chong, G.: The Precordilleran fault system of Chuquicamata, northern Chile: Evidence for reversals along arc-parallel strike-slip faults, Tectonophysics, 259, 213-228, 10.1016/0040- 1951(95)00109-3, 1996.

Riesner, M., Lacassin, R., Simoes, M., Carrizo, D., and Armijo, R.: Revisiting the crustal structure and kinematics of the Central Andes at 33.5°S: implications for the mechanics of Andean mountain-building, Tectonics, 10.1002/2017TC004513, 2018.

Riesner, M., Lacassin, R., Simoes, M., Armijo, R., Rauld, R., and Vargas, G.: Kinematics of the active West Andean fold-and-thrust belt (Central Chile): structure and long-term shortening rate, Tectonics, 36, 10.1002/2016TC004269., 2017.

Rosu, A.-M., Pierrot-Deseilligny, M., Delorme, A., Binet, R., and Klinger, Y.: Measurement of ground displacement from optical satellite image correlation using the free open-source software MicMac., ISPRS Journal of Photogrammetry and Remote Sensing, 100, 48-59, 10.1016/j.isprsjprs.2014.03.002, 2014.

Rupnik, E., Pierrot-Deseilligny, M., Delorme, A., and Klinger, Y.: Refined satellite image orientation in the free open-source photogrammetric tools Apero/Micmac, ISPRS Annals of Photogrammetry, Remote Sensing and Spatial Information Sciences, 3, 83-90, 10.5194/isprs-annals-III-1-83-2016, 2016.

SERNAGEOMIN: Mapa Geológico de Chile: versión digital., Servicio Nacional de Geología y Minería, Publicación Geológica Digital, Santiago, Chile, 2003.

Sheffels, B. M.: Lower bound on the amount of crustal shortening, in the central Bolivian Andes, Geology, 18, 812-815, 10.1130/0091-7613(1990)018<0812:LBOTAO>2.3.CO;2, 1990.

Skarmeta, M. J. and Marinovic, S. N.: Geologia de la hoja Quillagua : Region de Antofagasta, escala 1:250.000., Instituto de Investigaciones Geologicas (Chile), Carta Geologica de Chile, 1981.

Steinmann, G.: Geologie von Peru, The Journal of Geology, 38, 10.1086/623704, 1930.

Suppe, J.: Geometry and kinematics of fault-bend folding, American Journal of science, 283, 684-721, 1983.

Tassara, A., Götze, H.-J., Schmidt, S., and Hackney, R.: Three-dimensional density model of the Nazca plate and the Andean continental margin, Journal of Geophysical Research: Solid Earth, 111, 10.1029/2005JB003976, 2006.

Tomlinson, A. J. and Blanco, N.: Structural evolution and displacement history of the West Fault System, Precordillera, Chile: Part 2, postmineral history, VIII Congreso Geológico Chileno, Antofagasta, Chile, 1878-1882,

Tomlinson, A. J. and Blanco, N.: Structural evolution and displacement history of the West Fault system, Precordillera, Chile: Part 1, synmineral history, VIII Congreso Geológico Chileno, Antofagasta, Chile, 1873-1877,

Tomlinson, A. J., Blanco, N., and Ladino, M.: Carta Mamiña, Región de Tarapacá., Servicio Nacional de Geología y Minería, Serie Geología Básica, 2015.

Tomlinson, A. J., Blanco, N., Maksaev, V., Dilles, J., Grunder, A. L., and Ladino, M.: Geología de la Precordillera Andina de Quebrada Blanca e Chuquicamata, Regiones I y II (20° 30' - 22°30'S), Servicio Nacional de Geología y Minería, Santiago, Chile, 444, 2001.

Vergara, H. and Thomas, A.: Hoja Collacagua: región de Tarapaca: carta geológica de Chile 1: 250.000., Servicio Nacional de Geología y Minería, 1984.

Victor, P., Oncken, O., and Glodny, J.: Uplift of the western Altiplano plateau: Evidence from the Precordillera between 20° and 21°S (northern Chile), Tectonics, 23, 10.1029/2003TC001519, 2004.

Wölbern, I., Heit, B., Yuan, X., Asch, G., Kind, R., Viramonte, J., Tawackoli, S., and Wilke, H.: Receiver function images from the Moho and the slab beneath the Altiplano and Puna plateaus in the Central Andes, Geophysical Journal International, 1040   177, 296-308, 10.1111/j.1365-246X.2008.04075.x, 2009.

Yuan, X., Sobolev, S. V., Kind, R., Oncken, O., Bock, G., Asch, G., Schurr, B., Graeber, F., Rudloff, A., Hanka, W., Wylegalla, K., Tibi, R., Haberland, C., Rietbrock, A., Giese, P., Wigger, P., Röwer, P., Zandt, G., Beck, S., Wallace, T., Pardo, M., and Comte, D.: Subduction and collision processes in the Central Andes constrained by converted seismic phases., Nature, 408, 958-961, 10.1038/35050073, 2000.

1045   Zandt, G., Velasco, A. A., and Beck, S. L.: Composition and thickness of the southern Altiplano crust, Bolivia, Geology, 22, 1003-1006, 10.1130/0091-7613(1994)022<1003:Catots>2.3.Co;2, 1994.

Zehnder, A. T. and Allmendinger, R. W.: Velocity field for the trishear model, Journal of Structural Geology, 22, 1009-1014, 10.1016/S0191-8141(00)00037-7, 2000.

1050